EVALUATION OF INTERNAL FIN GEOMETRY FOR HEAT TRANSFER ENHANCEMENT IN AUTOMOBILE EXHAUST ENERGY HARVESTING SYSTEMS

Jayati D. Athavale

Thesis submitted to the faculty of the Virginia Polytechnic Institute and State University in partial fulfillment of the requirements for the degree of

Master of Science

in

Mechanical Engineering

Srinath V. Ekkad

Scott T. Huxtable

Brian Vick

December 5, 2013

Blacksburg, VA

Keywords: Heat Transfer enhancement, Heat exchanger, Louvered fins, Herringbone wavy fins, Thermoelectric generation, TEG

Evaluation of Internal Fin Geometry for Heat Transfer Enhancement in Automobile Exhaust Energy Harvesting Systems

Jayati D. Athavale

Abstract

Thermoelectric generators (TEGs) are currently being explored for their potential in harvesting energy from automobile exhaust. TEGs in form of an appropriate TEG- Heat exchanger module can utilize the temperature difference between the hot exhaust gases and the automobile coolant and convert it into electrical voltage. The amount of power is anticipated to be a few hundred watts depending on the temperature gradient and the material of the TEGs.

The focus of this study is increasing the hot side heat transfer for improved performance of the thermoelectric generators using two different internal fins – louvered fins and herringbone wavy fins. The multi-louvered fins basically have 'multi flat plate' behavior and will enhance the heat transfer by deflecting the air from its original path and aligning it with the plane of the louvers. Herringbone fins are used to lengthen the path of airflow allowing for greater residence time and better mixing of the flow. They also provide for greater wetted surface area achieving higher heat transfer. The flow and heat transfer behavior inside the exhaust pipe test section with internal fins is modeled using commercial numerical software.

The thermal and flow behavior through both these internal fins depends to a large extent on geometric parameters and fin arrangement. Optimization of the fin design is considered to determine the configuration that provides highest heat transfer while providing least pressure drop across the pipe length. The heat transfer and pressure drop characteristics are compared to the baseline flow without any fin enhancement.

To my Family & Friends

Acknowledgements

I would like to express my deepest gratitude to my advisor Dr. Srinath Ekkad for extending this opportunity of working in his lab and conducting my masters research under his guidance. I have truly appreciated his advice and guidance in matters regarding my project as well as other personal decisions. His enthusiasm was always an inspiration to me. I would also like to thank Dr. Huxtable for many hours that he spent with us in meetings and for all the advice.

This research is based upon the work supported by the National Science Foundation and Department of Energy through an NSF/DOE Joint Thermoelectric Partnership, Award Number CBET-1048708. I would like to thank both the NSF and the DOE for their support of this project.

I would like to thank all my lab mates for their support, cooperation and a great working environment. I would especially like to thank Jaideep Pandit who has been a great support .He was always available for expert advice, constructive criticism and much needed encouragement.

I would like to thank my parents, my sister, and all my friends and family for their constant encouragement, care and belief in me. I would especially like to thank my aunt and uncle, Mrs. Anjali and Mr. Dattatraya Gokhale who have had an indispensable contribution in my life.

Last but not the least I would like to thank my friends here for the countless hours they have spent reading my thesis and patiently listening as I practiced my presentation, not understanding most part of it but still appropriately nodding. You guys made everything much easier.

TABLE OF CONTENTS

LIST OF FIGURES

LIST OF TABLES

NOMENCLATURE

A = cross-sectional area of the exhaust pipe section (m^2)

D = ideal transverse distance travelled by streak line (m)

D_h = hydraulic diameter (m)

F_d = fin depth (m)

F_p = fin pitch (m)

h = heat transfer coefficient (W/m^2K)

F_l = fin length (m)

k = thermal conductivity (W/mK)

L_h = louver height (m)

L_l = louver length (m)

N = actual transverse distance travelled by streak line (m)

Nu = Nusselt number (-)

P = power generated by TEG (watts)

PEF = performance enhancement factor (-)

Δp = pressure drop across the fins (Pa)

Q = heat supplied to the TEG (watts)

Re = Reynolds number based on hydraulic diameter (-)

Re_{Lp} = Reynolds number based on Louver pitch (-)

$Re *_{Lp}$ = critical Reynolds number (-)

S = half-length of inlet deflection louver ($= Lp/2$) (m)

St = Stanton number (-)

t = fin thickness (m)

T = absolute Temperature (K)

ΔT = temperature differential (K)

V = voltage (Volts)

W_p = wave pitch for wavy fins (m)

Δy = first layer thickness (mm)

Y^+ = non dimesional distance from the wall (-)

Z = performance parameter of thermoelectric material (K^{-1})

ZT = Figure of merit for thermoelectric material (-)

Greek symbols

α = Seebeck coefficient (Volts/K)

η = flow efficiency (-)

η_{TEG} = efficiency of the TEG (-)

θ_l = louver angle (degrees)

θ_w = wavy angle (Degrees)

Subscripts

l = louvered fin

w = herringbone wavy fins

h = hot side

c = cold side

in = inlet conditions

out = outlet conditions

0 = baseline case

CHAPTER 1: INTRODUCTION

The transportation industry and the use of automobiles have exponentially grown in the last few years leading to an increase in consumption of the already scarce fossil fuels[1]. Efficient utilization of energy content of fuels is therefore of paramount importance. Under normal operating conditions, out of the total energy obtained from the combustion of fuel only 25% is used to drive the vehicle and the electrical accessories, while 40% is lost in the form of exhaust gases[2-5]. Thermoelectric generator (TEG) modules are currently being investigated for their potential to recover part of the energy of the exhaust gases. Even if only 6% of the heat from the exhaust gas could be harnessed by the use of TEG, it could lead to a reduction in fuel consumption by around 10% which is significant in terms of the present global fuel economy[6]. Current estimates for the improvement of the fuel economy in a car using TEG modules are 2 to 5% [2].

Energy recovery using TEG modules can be maximized by developing thermoelectric materials with improved properties and having efficient heat transfer to and from the TEG. However, improving the material properties can reach the efficiency to only 50% of the stated Carnot efficiency [2, 3]. To improve the efficiency beyond this focus must be directed towards enhancing the heat transfer process to and from the TEG.

This study focuses on numerical analysis to maximize heat transfer to the hot side of the thermoelectric generator module. Two heat exchanger designs with different internal fins – louvered fins and herringbone wavy fins have been considered. Geometry optimization for both the fins has been carried out to reach a design which gives highest heat transfer enhancement compared to the baseline case without any internal fins. Trends for heat transfer and pressure drop as a function of the varying geometric parameters have been obtained and can be used for design of similar heat exchangers. The computational domain is $1/5^{th}$ scale of the actual module in an automobile. All the scaling is based on Reynolds number. The temperatures used for the hot side and the exhaust are typical of the engine conditions.

1.1 Thermoelectric generators:

The working of thermoelectric generators is based on a physical phenomenon called Seebeck effect. In general there is a relation between how most metals and semiconductors conduct heat energy and electrical energy. Electrons haul the electrical energy with them when they carry heat energy. Thus if a temperature gradient is applied to a thermoelectric material , as heat flows from higher temperature to lower temperature, electrons also diffuse from the hot side to the cold side. These free electrons are deposited onto the cold side. This diffusion of electrons generates electric potential that can be tapped and used to power electrical auxiliaries. Thus thermoelectric generators can be used to convert available temperature differential into electrical energy. The following equation relates the electrical voltage produced by TEG to the temperature gradient supplied to it [4]:

$$V = \alpha \Delta T \tag{1.1}$$

Thermoelectric materials, that form the crux of the TEG, demonstrate the Seebeck effect in a strong or convenient form. They are characterized by a parameter called figure of merit used to compare different thermoelectric materials suitable for TEGs. Figure of merit takes into account the Seebeck coefficient α, the average absolute temperature of the material, T, the electrical resistivity, ρ, and the thermal conductivity of the material k. It is given by:

$$ZT = \frac{\alpha^2 T}{\rho k} \tag{1.2}$$

An ideal thermoelectric material has high figure of merit because of high value of Seebeck coefficient and low value of electricity resistivity.

Electrical power generated by a TEG is given by:

$$P = \eta_{\mathrm{TEG}} Q \tag{1.3}$$

Where, η_{TEG} is the efficiency of the thermoelectric generator and Q is the heat applied to the TEG. The main aim of the project is to employ a TEG to harness the heat energy from the exhaust gases in the form of electrical power. As such the power produced by TEG is an important consideration, which increases as the efficiency of TEG increases. Equation (4) calculates the efficiency of the TEG.

$$\eta_{\mathrm{TEG}} = \frac{\Delta T}{T_h} \cdot \frac{\sqrt{1 + \overline{ZT}} - 1}{\sqrt{1 + \overline{ZT}} + T_c / T_h} \tag{1.4}$$

Thus the efficiency is dependent on the temperature gradient across the TEG, ΔT, the figure of merit, ZT, the hot side and cold side temperature, T_h and T_c respectively. It can be seen from the equation (4) that efficiency of TEG increases with increase in temperature gradient. For every degree kelvin rise in the temperature differential, the efficiency increases by around 0.04%. [6]Improving T_h as seen by the TEG is important in this respect. Higher value of T_h will result in an increase inΔT. This would improve the efficiency of the TEG module and result in higher power generation.

1.2 TEG – Heat Exchanger Model:

Figure 1.1 gives the baseline TEG- Heat exchanger model used for this study that has been designed by Pandit, et al.[7]. The model is basically made up of three distinct parts as follows:

i. The rectangular pieces are the **TEG units** which convert the supplied temperature difference into electricity.

ii. The gray section is the **hot side loop** which provides the hot side temperature for the TEGs. It is an open loop that comprises of the exhaust gas pipe.

iii. The brown section is the **cold side loop** and it provides for the cold side temperature for the TEGs. It is a closed loop that carries the automobile coolant.

Of these the hot side and cold side loop comprise the heat exchanger part of the model. As seen from the figure the heat exchanger unit is built around a flattened section of the exhaust tail pipe. The top and the bottom part of the exhaust pipe are flattened so that TEGs could be easily placed onto it. The coolant loop completely envelopes around the hot exhaust pipe as well as the TEGs.

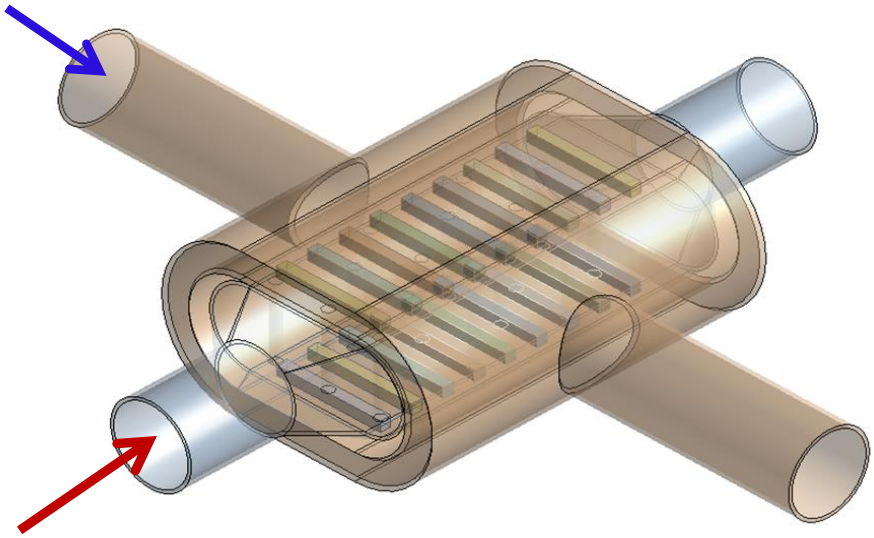

Fig. 1.1: Baseline TEG-Heat exchanger module

Figure 1.2 shows the front view of the TEG – Heat exchanger module. It can be seen that the hot side loop and the cold side loop carry the exhaust gases and the coolant respectively in mutually perpendicular directions like in a cross flow heat exchanger. In this view hot exhaust gases flow into the plane, while the arrows represent the direction of the coolant flow. The TEG units are sandwiched between both the loops with one of their surfaces in contact with the exhaust pipe (hot loop) while the other with the coolant pipe (cold loop). Thus for the TEGs the exhaust pipe wall temperature represents the hot junction temperature while the coolant pipe temperature represents the cold junction temperature.

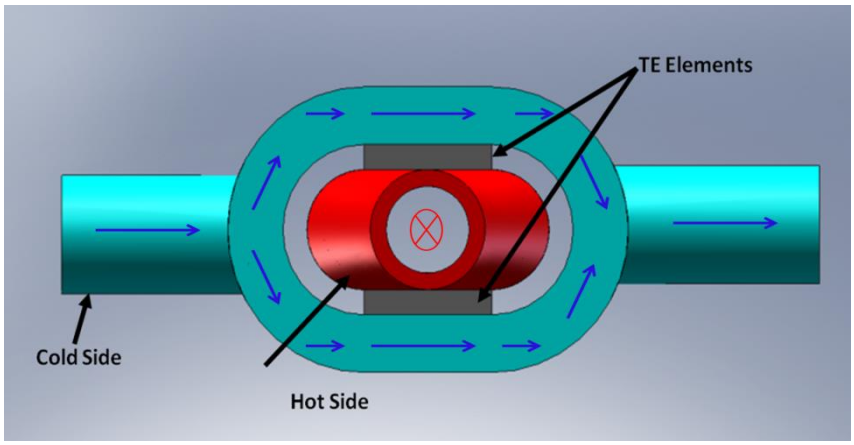

Fig.1.2: Front view of TEG- Heat Exchanger module

1.3 Hot Loop Heat Transfer Enhancement:

As stated earlier, for thermoelectric module, the hot side temperature T_h comes from the hot exhaust gases. The temperature of the exhaust gases, which is a limiting case for hot side temperature T_h, is fixed by the combustion process and the engine running conditions, and hence cannot be controlled or increased. Thus the next best option is to develop a design so that hot side temperature approaches the exhaust gas temperature as closely as possible. Internal fins incorporated in the exhaust pipe test section are explored as an option to achieve this. Thus the main objective of this study is to maximize the energy of exhaust gases that is transferred to the exhaust pipe wall. . In a heat exchanger that employs a gaseous working fluid, up to 80% of the total thermal resistance is due to the gas side [8]. In the TEG module under discussion, the hot side has the exhaust gases as a working fluid. The thermal resistance on the hot side can be decreased by employing internal finned surfaces and thus, achieve better heat transfer performance of the heat exchanger. Two types of internal fins are considered- Louvered fins and Herringbone wavy fins. Both of these fins are passive heat transfer augmentation techniques. They do not need any external power input and any additional power needed to enhance the heat transfer is taken from the available power in the system. This ultimately leads to a higher pressure drop in the system.

These fins achieve heat transfer enhancement by altering or disturbing the existing flow behavior. The basic geometry for both these fins is explained in the following sections.

1.4 Louvered Fins

Figure 1.3 borrowed from Ref . [9] explains the basic structure of the louvered fins. Each slanting strip is termed as a louver and all the louvers in any one horizontal line comprise a fin. The distance between adjacent louvers in a fin is the louver pitch and the distance between adjacent fins is the fin pitch. The angle that the louvers make with the span wise direction is termed as the louver angle. Some non-dimensional parameters defined in the literature for louvered fins are as follows - ratio of the louver pitch to fin pitch (Lp/Fp) and the ratio of fin thickness to louver pitch (t/Lp). For flow through louvered fins Reynolds number can be defined in different ways depending on the dimension used for the characteristic length. It can based off hydraulic diameter (Re_{Dh}), fin thickness(Re_t), fin

pitch (Re_{Fp}), or the louver pitch(Re_{Lp}). Louvered fins can be manufactured by high speed production techniques and hence are less expensive than other interrupted flow geometries when produced in large quantities. Louver strips are generally formed by cutting the metal and pushing out the cut elements from the plane of the base metal.

Louvered fins cause heat transfer augmentation by increase in surface area and introduction of secondary flow phenomenon. Additionally because of the corrugated nature of louvered fins there is continuous growth and destruction of laminar boundary layers.

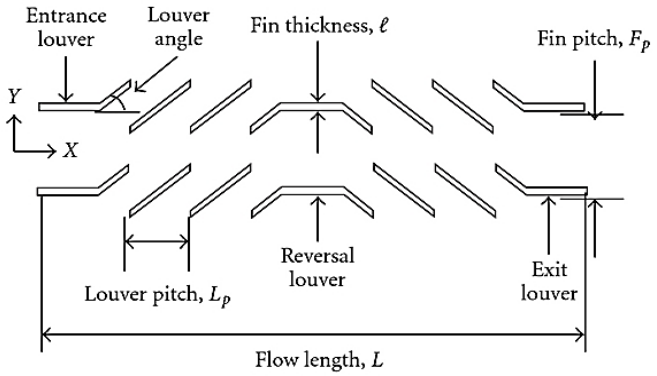

Fig.1.3: Basic multi- louver fin geometry

1.5 Herringbone Wavy Fins:

Figure 1.4 explains the basic geometry of the Herringbone wavy fins. Slant length (s) represents the length of the slant face of the triangular fins. Wavy angle (θ_w) is the inclination of the triangular faces with the horizontal. Wave pitch gives the distance between corresponding points on consecutive corrugations. Wave pitch (W_p) is a direct function of the wavy angle θ and the Slant length (s)and is directly related by:

$$W_p = 2s\ cos\theta_w \tag{1.5}$$

Fin Pitch (F_{pw}) gives the distance between successive fins. The fin thickness (t_l) represents the thickness of the metal strip used to construct the fins.

Corrugated or wavy fins lengthen the path of flow thus increasing the residence time of the fluid in the channel. Moreover, due to the corrugated geometry of the fins, the fluid is periodically deflected from its flow path as it continuously tries to be aligned with the fin faces. This causes separation and reattachment of the thermal boundary layer resulting in higher convective heat transfer. Also, flow visualization experiments by Ali and Ramadhyani [10] have shown that at higher Reynolds number ($Re > 650$) stream wise (Goertler) and span wise vortices occur which causes local heat transfer coefficient to increase.

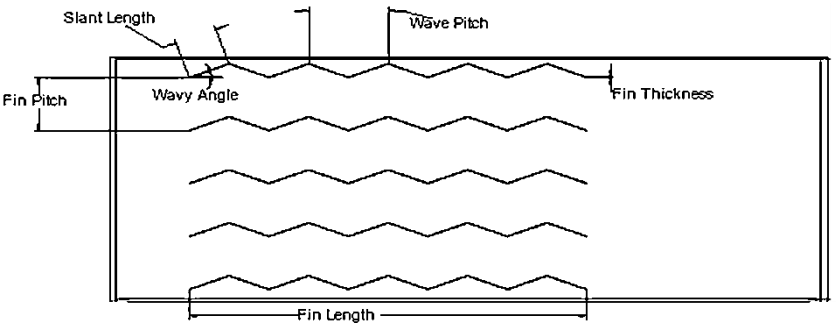

Fig. 1.4: Basic geometry of herringbone wavy fins

The following two chapters, chapter 2 and 3, individually deal with the two types of internal fins and include the literature review, the computational set up and the results and discussion. For the purposes of geometry optimization of the internal fins the exhaust pipe section is modelled as a rectangular pipe. This allows for easier manipulation of the geometric features of the internal fins. Additional simulations are conducted to ensure that the results and trends obtained for the internal fins in the simplified rectangular channel with uniform inlet velocity are valid and applicable for the exhaust pipe section with diverging entrance region as seen in figure 1.1. The results and set up for these are included in chapter 5.

CHAPTER 2: LOUVERED FINS

2.1 Literature Review:

Several studies on thermal and hydraulic characteristics of flow through louvered fins have been reported in literature. However, most of these studies discuss louvered fins as part of the cross flow fin and tube heat exchanger and not as a stand-alone unit. The first reported flow visualization experiments have been done by Beauvais [11] in 1965 using smoke flame visualization technique with 10:1 scale models. Though the results for his experiments have not been quantified, in the sense that geometric dimensions and velocities were not documented in his paper (From close observation of his pictures it is generally accepted that the louver angle was approximately $30°$ and the louver to fin pitch ratio (Lp/Fp) was approximately 0.80.), the pictures from his study have been the first to indicate that the main flow was aligned with the louvers for the velocities tested. Prior to this work, it was believed that louvers acted as surface roughness that enhanced heat transfer by promoting turbulence only.

In 197 Wong and Smith [12] experimentally determined nusselt number and drag coefficient for a 5:1 scale model of a louvered fin array. The results were in agreement with similar full- scale louvered fin arrays for the same Reynolds number and they therefore concluded that the air flow phenomenon was the same for the full scale and model cores. In 1980, Davenport [13] using the smoke tracer technique involved 32 samples of non-standard variant of triangular louvered fins. He demonstrated that the degree of alignment with the louvers was a function of the Reynolds number(Re_{Lp}). At low values of Re_{Lp}, the flow was predominantly axial (duct directed) with very little effect of the louvers. However, at higherRe_{Lp}, most of the flow is parallel to the louvers (louver directed flow). Figure 2.1[13] makes this phenomenon clear.

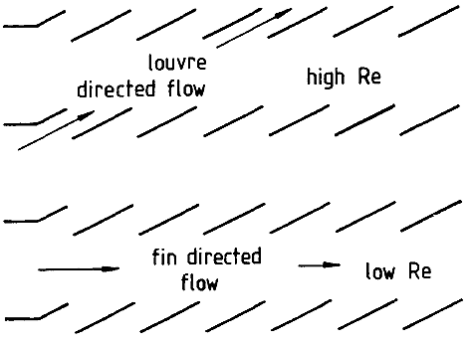

Fig. 2.1: Fin directed and louver directed flow

Achaichia and Cowell [14] reported one of the first numerical studies for fully developed periodic flow situation in 2D louvered fin array. Figure 2.2 taken from Ref. [14] shows the variation of mean flow angle with Re_{Lp}. At low Re_{Lp} the mean flow angle is significantly smaller than the angle louver, which it approaches as the Re_{Lp}goes on increasing.

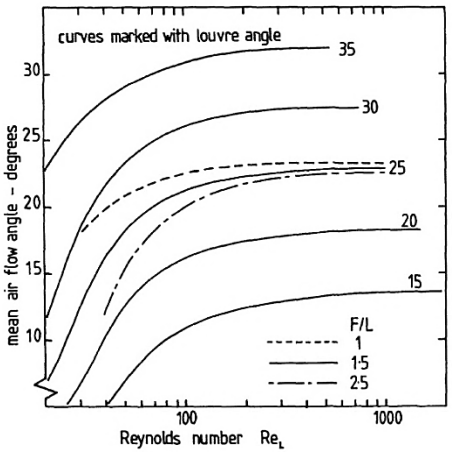

Fig. 2.2: Variation of mean flow angle with Re_{Lp}

Extensive experiments have been conducted by Webb and Trauger [15] to investigate the flow phenomenon in a louver array and to determine the effect of velocity and geometrical parameters on the flow structure. The flow visualization model selected was a 10: l scaled up model satisfying the geometric and dynamic similarity and had $Lp/Fp, Lp/t$ and θ_l typical of common industrial designs. Figure 2.3 taken from Ref. [15] explains flow efficiency for louvered fins as defined in this study:

$$\eta = \frac{N}{D} = \frac{Actual\ transverse\ distance}{Ideal\ transverse\ distance} \tag{2.1}$$

The flow efficiency can be viewed as the ratio of the mean flow angle to the louver angle.

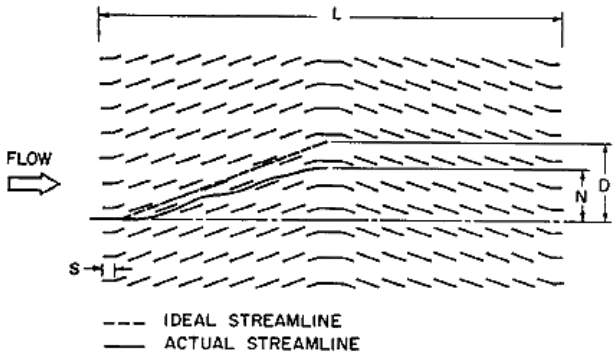

Fig. 2.3: Method of defining flow efficiency

The authors concluded that louvered fin efficiency increases with an increase in θ_l till a certain critical Reynolds number($Re*_{Lp}$) beyond which it is independent of the louver angle. Fin efficiency also increases with an increase in Re_{Lp} and the ratioL_p/F_{pl}. This can be seen from fig.2.4 borrowed from Ref. [15].

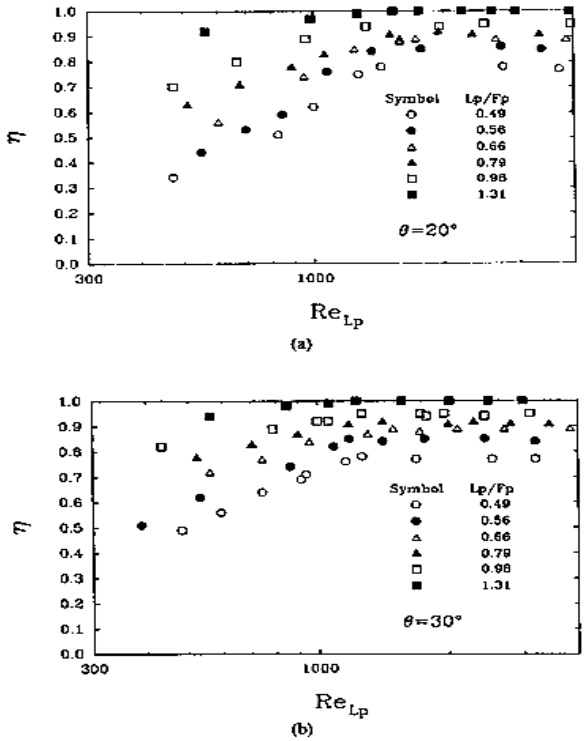

Fig. 2.4: (a) Flow efficiency versus $Re_{Lp}$for $\theta_l = 20°$ (b) Flow efficiency versus $Re_{Lp}$for $\theta_l = 30°$

Relation between flow efficiency and geometrical parameters was studied by Zhang and Tafti [16-17] using numerical methods .It was reported that the flow efficiency increases with increase in Reynolds number and louver angle and decrease in fin pitch and thickness ratio. CFD studies by Suga and Aoki [18] aimed at optimizing the louver pitch to fin pitch ratio. They predicted the optimum to occur when a line can be extended from the trailing edge of the louver to reach the mid-point between the next pair of downstream louvers. Numerical simulations for performance of louvered fin array were conducted by Perrotin and Clodic [19] using 2D and 3D models. The results for the two models were compared to the available experimental data bank and correlations. The authors found that 2D models over predict the heat transfer coefficient by up to 80%. 3D models however account for fin thermal conductivity and hence match much more closely to experimental data (13%).

The present research is focused on investigating the flow and thermal behavior in a channel with internal louvered fins for a specific application. As such the geometric configurations considered are

unique and hence, the results cannot be directly compared to those available in the literature. However, the trends have been analyzed and they compare well with the previous studies.

The following sections deal with the description of the physical test geometry of the exhaust pipe as well as the internal louvered fin configuration .The computational set up including the domain discretization, boundary conditions, turbulence model and grid independence is also discussed. In the results section the trends obtained for heat transfer and pressure characteristics are analyzed and compared to the baseline case with no fins. Performance of the various configurations is compared by considering the performance enhancement factor that characterizes the enhancement in heat transfer achieved and the associated pressure drop increment in the system.

2.2 Geometry Description:

2.2.1Exhaust Pipe Section:

For the CFD analysis and concept validation of the internal louver fin geometry simplified rectangular test section is considered. Figure 2.5 show the rectangular test section with internal louvered fins. The part of the rectangular exhaust pipe having internal louvered fins is 0.3m long with the cross-section being 0.18m x 0.0714m. The thickness of the exhaust pipe is 0.003m. The hydraulic diameter $(4A/P)$ for this cross-section comes out to be 0.1025m The section of the pipe has been extended on both sides of the actual test section to facilitate initial flow development and to prevent backflow.

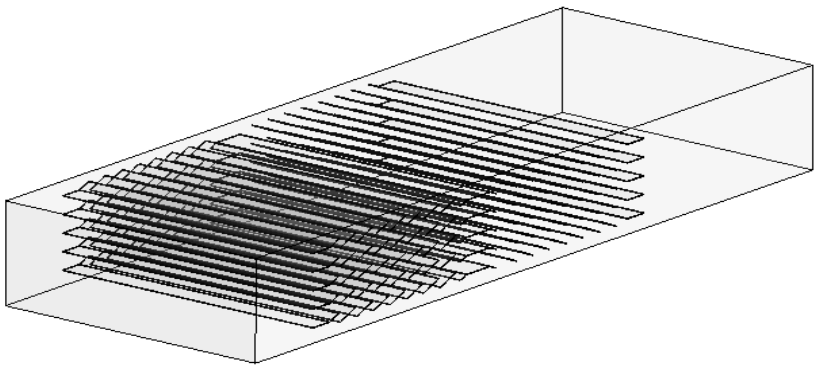

Fig. 2.5: Exhaust pipe test section with internal louvered fins

2.2.2 Internal Louvered Fin Geometry:

The basic geometry of the louvered fins has been explained in the introduction section. Heat transfer and pressure drop characteristics have been analyzed for variation in three parameters – ratio of louver pitch to fin pitch L_p/F_{pl}, louver angle θ_l and the flow Reynolds number. While varying the geometric parameters, the exhaust pipe dimensions have been taken to be fixed. The louver pitch has been taken to be the fundamental dimension and the value of the fin pitch is decided on the basis of the required L_p/F_{pl} ratio. Three values of the louver pitch L_p have been tested: 12.5mm, 15mm and 17.5mm. These are in range of typical values in contemporary industrial designs. This allows for computational analysis of the louvered fins for L_p/F_{pl} ratio in the range of 0.9 – 1.84, the other parameters being held constant. In most studies till date L_p/F_{pl} ratios greater than 1.5 have not been tested. The louvered angles being tested are $-20°, 25°$ and $30°$ and the flow has been tested for Reynolds number of 10000, 20000 and 30000, which are all in the turbulent regime.

The thickness of the louvers is kept constant for all cases. The horizontal parts of the entrance and exit louver are taken to be equal to L_p.The length of the reversal louver has been decided subject to the uniform spacing between the louvers (louver pitch) for each configuration.

Table below gives a summary of the basic dimensions:

Table 2. 1 Geometrical parameters for test section with louvered fins

Parameter	Value
Length of test section(L)	0.5m
Width of test section(W)	0.181m
Height of test section(H)	0.0714m
Fin thickness	0.0005m
Louver Pitch	12.5mm/15mm/17.5mm
Louver angle	$20°/25°/30°$
Lp/Fp	09-1.84

2.3 Computational Set up:

The Computational Fluid Dynamics analysis has been carried out using commercial CFD code Ansys CFX 13.0 module. The geometry has been divided into two domains; the solid domain consisting of the exhaust pipe structure and the louvered fins, and the fluid domain through which the exhaust gases flow. Thus it is a conjugate heat transfer model accounting for convection inside the fluid domain as well as conduction within the fins and the exhaust pipe shell.

2.3.1 Domain discretization and Mesh:

Both the solid as well as the fluid domains have been discretized using the finite volume method. The grid was unstructured and comprised of tetrahedron, pyramid and wedge shaped cells. The mesh has been created using the patch conforming method which used a bottom-up approach (creating the surface mesh and then the volume mesh). Body sizing functions have been used to specify the grid size to maintain control over the refinement, smoothness and quality of the mesh. Figure. 2.6(a) shows a representation of the mesh.

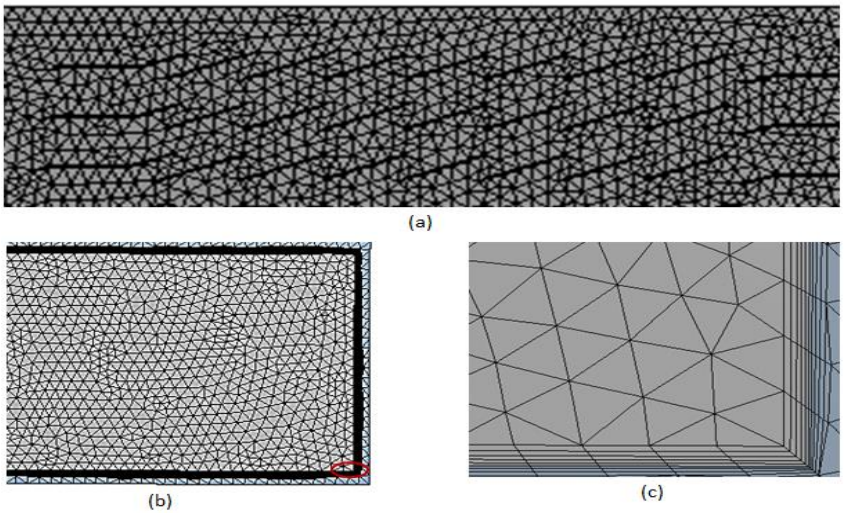

Fig 2.6: (a) Top view, patch conforming mesh (b) Discretization of the fluid and solid domain with inflation layers at the interface (c) Enlarged inflation layers

Inflation layers have been used on the solid-fluid interface (inner walls) of the exhaust pipe to capture the velocity and temperature variations in the boundary layers. The first layer thickness for the inflation layers has been calculated based off on a y+ value of 1, which is typical for the Shear Stress Transport (SST) model to ensure that the laminar sub layer is captured. Five inflation layers have been

considered with a growth rate of 1.2. Figure 2.6(b) shows the inflation layers on the solid fluid interface and Fig. 2.6(c) shows the exaggerated view of the same.

2.3.2 Turbulence model:

For all the three Reynolds number chosen the flow inside the exhaust pipe was turbulent. Industrial standard Shear Stress Transport (SST) model was employed to model the turbulence. The model uses the turbulence-based k- ω model at the wall and the k- ε model in the bulk flow with an automatic intermediate blending function that ensures a smooth transition between the two models[20]. It has been shown by studies that the solutions based on SST model are largely insensitive to the near wall grid resolution. The heat transfer from the fluid to the wall and thermal profile of the wall was an important metric for this study hence the SST model was found suitable.

2.3.3 Boundary Conditions:

It has been found that as an approximation, the properties of air can be used for exhaust gas calculations [21] and the error associated with neglecting the combustion products is usually no more than about 2%. Hence, for simplicity, the working fluid has been taken to be air with ideal gas properties. For the fluid domain, a uniform velocity and temperature type boundary condition has been applied at the inlet while the outlet had a pressure type boundary condition that was set to atmospheric pressure. The inlet velocity was calculated based on the desired Reynolds number and the temperature of the incoming exhaust gases was taken to be 700K for all cases.

The material of the exhaust pipe and the fins (solid domain) is taken to have properties of steel. The outside of the exhaust pipe wall is modeled by applying a constant outgoing heat flux equal to $1000\ W/m^2$.

2.3.4 Grid Independence:

Grid independence study was conducted for the computational domain. Starting from a coarse mesh the grid was systematically refined till the results were within acceptable variation compared to the previous mesh. The two important metrics for this study are the exhaust pipe wall temperature and the pressure drop in the channel. Mesh was taken to be optimum when the solution for both of these metrics was independent of the grid.

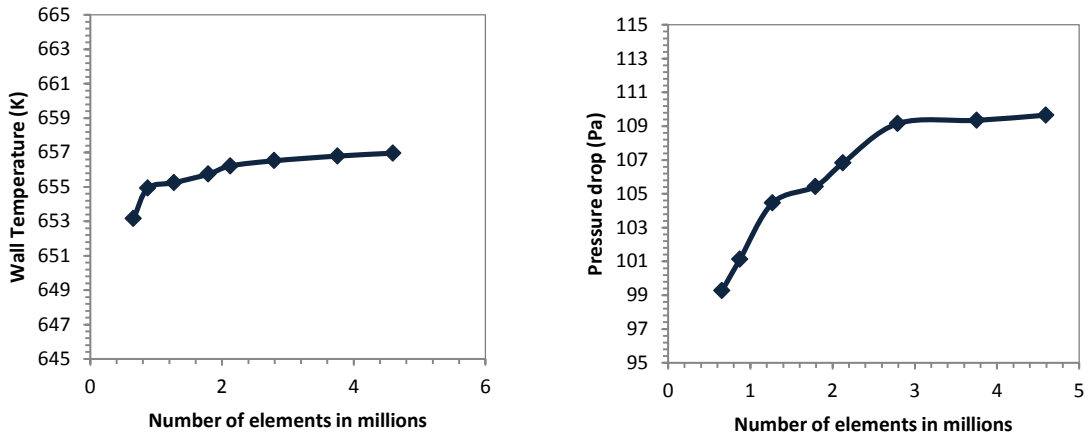

Fig. 2.7: Variation in wall temperature and pressure drop with number of elements

Figure 2.7 shows the curves for grid independence. Based on this, a grid with 2.8 million elements was taken to be sufficiently resolved. Beyond this mesh size the variation in pressure and temperature measurements was found to be within 0.37% and 0.06% respectively.

2.4 Results and Discussions:

Numerical simulations are performed to characterize the heat transfer and pressure drop in the exhaust pipe test section. The quantities of interest are the exhaust pipe wall temperature and the total pressure drop along the test section. Higher wall temperature is indicative of more heat being transferred from the exhaust gases to the walls and hence relates to higher heat transfer coefficient. Results are presented as normalized pressure drop and normalized wall temperature as follows:

$$P^* = \frac{\Delta p}{\Delta p_0} \tag{2.2}$$

$$T^* = \frac{T_{in} - T_0}{T_{in} - T_w} \tag{2.3}$$

For the baseline case, $P^* = T^* = 1$.

The average heat transfer coefficient is given by:

$$h = \frac{\dot{q}}{(T_b - T_{w,avg})} \tag{2.4}$$

$\dot{q}$ is the applied heat flux boundary condition at the wall. The bulk fluid temperature is defined as:

$$T_b = \frac{T_{in} + T_{out}}{2} \tag{2.5}$$

$T_{w,avg}$ is the average surface temperature of the walls.

The Nusselt number is given by:

$$Nu = \frac{hD_h}{k_{air}} \tag{2.6}$$

The characteristic length is the hydraulic diameter which is computed as:

$$D_h = \frac{2HW}{(H + W)} = 0.1025 \tag{2.7}$$

Another important parameter used to compare the performance of different configurations of the louvered fins has been the performance enhancement factor (PEF).

$$PEF = \frac{(Nu/Nu_0)}{(\Delta p/\Delta p_0)^{1/3}} \tag{2.8}$$

As can be seen from the equation, PEF characterizes the heat transfer enhancement achieved for increased penalty in terms of pressure drop.

2.4.1 Flow in Louvered Fins:

As mentioned previously the efficiency of louvered fins depends on the degree of alignment of the flow with the louvers. The closer the mean flow angle approaches the louver angle the better are the heat transfer characteristics. Figure 2.8 shows streamlines for flow through louvered fin geometry. The flow is almost entirely louver directed as is seen from the Fig. 2.8.

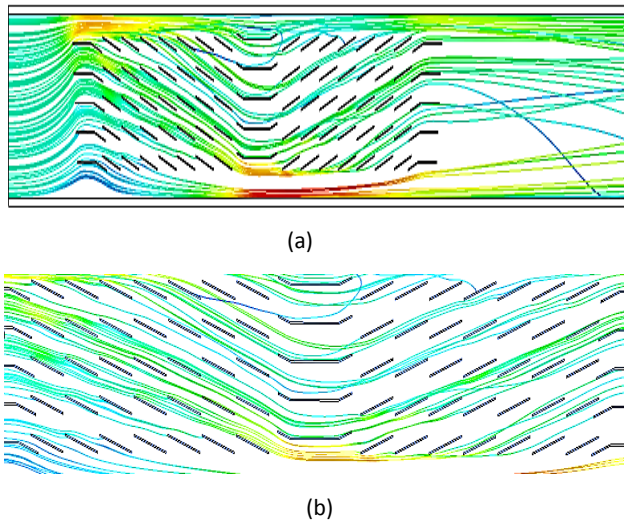

Fig. 2.8: Streamlines for flow through louvered fins

2.4.2 Contour Plots:

Figure 2.9 gives a representative comparison of wall temperature for the test section with louvered fins to the baseline case. The geometric parameters for this fin configuration are shown in the figure. The average wall temperature and heat transfer coefficient for the test section with the herringbone fins is 647.69K and $20.335\,W/m^2$while for the baseline case is 626.7K and $14.28\,W/m^2$. This indicates the potential of louvered fins for heat transfer augmentation.

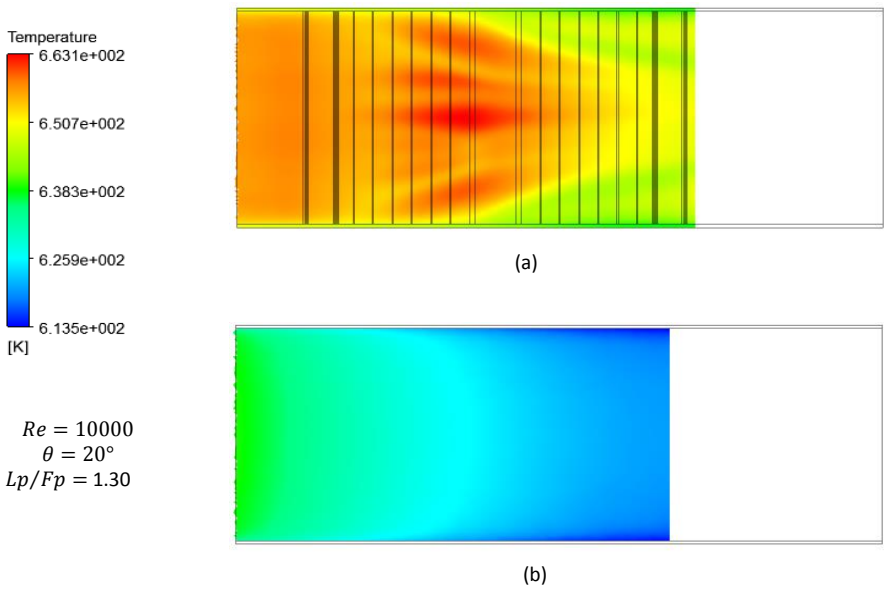

Fig.2.9: Comparison of wall temperature profile for louvered fins and baseline case

Figure 2.10 gives the comparison for the pressure drop for the louvered fins with the baseline case. The pressure drop for the test section with fins is 64.92Pa while that for the baseline case is 2.082 Pa. The performance enhancement factor for this particular case is 0.453.

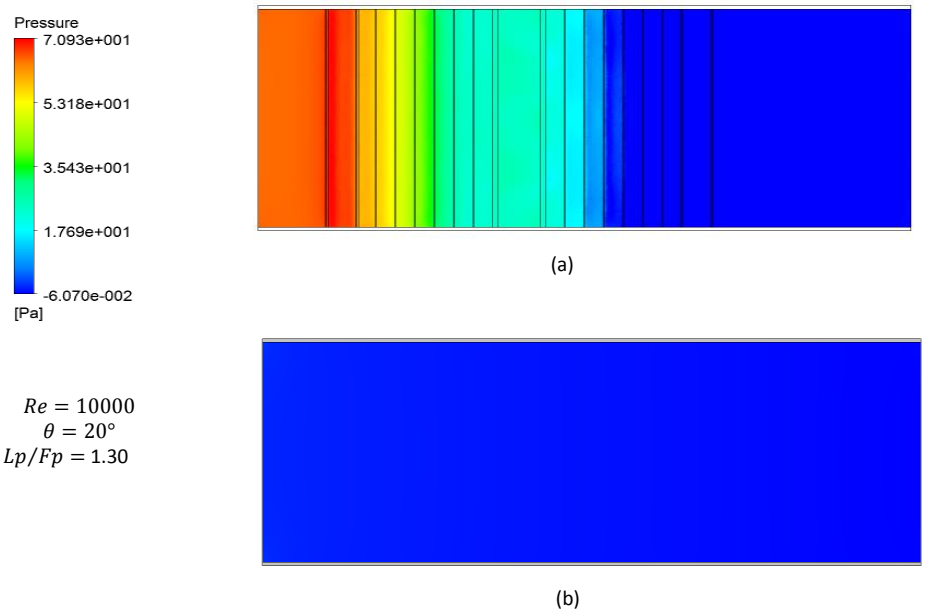

Fig.2.10: Comparison of pressure drop profile for louvered fins and baseline case

2.4.3 Effect of Varying Reynolds Number:

Heat transfer characteristics of louvered fins were investigated for three different Reynolds number (10000/20000/30000) while keeping the geometrical parameters fixed ($\theta = 25°, Lp/Fp = 1.305$).

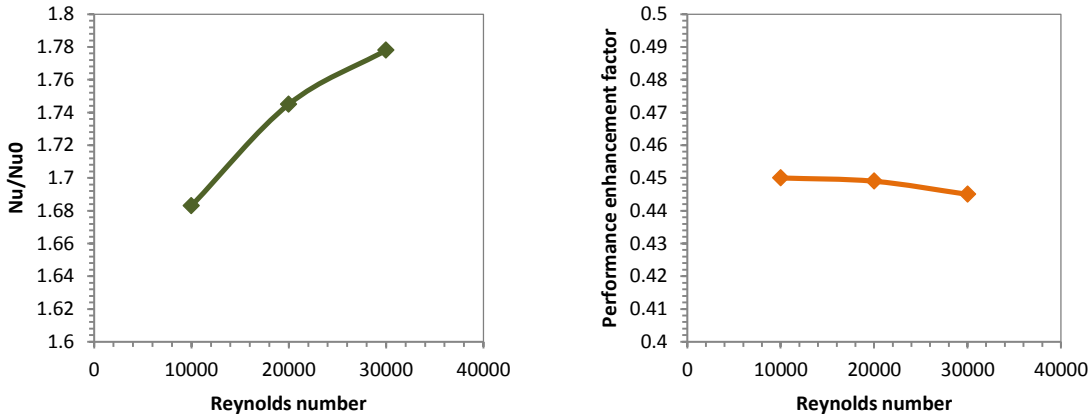

Fig. 2.11: (a) Variation in ratio Nu/Nu_0 with Reynolds number (b) Variation in PEF with Reynolds number

Relative Nusselt number is minimum for Re=10000 and it goes on increasing as Reynolds number increases as seen in Fig. 2.11(a). Thus as Reynolds number increases, heat transfer as well as heat transfer enhancement over the baseline case increases. This indicates that heat transfer characteristics of louvered fins are better at higher mass flow rates associated with high Reynolds number. Performance enhancement factor decreases slightly with Reynolds number as seen in Fig. 2.11(b). Figure 2.12 gives the normalized temperature and pressure drop as the Reynolds number is varied. It is seen that pressure drop with respect to the baseline case increases rapidly as the mass flow rate increases.

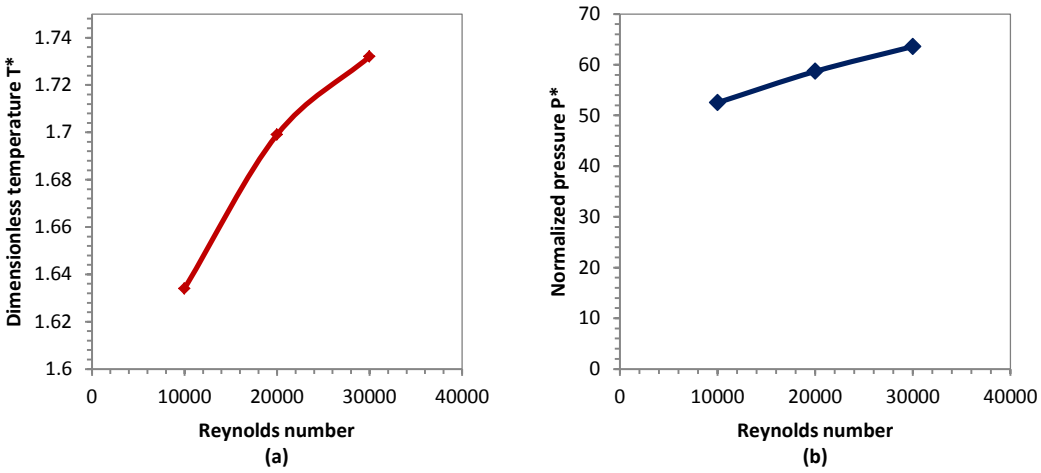

Fig.2.12: (a) Variation in dimensionless temperature with Reynolds number (b) Variation in normalized pressure drop with Reynolds number

2.4.4 Effect of Varying Louver Angle:

Figure 2.13(a) gives variation in relative nusselt number with varying louver angle, the other parameters remaining constant ($Lp/Fp = 1.305, Re = 10000$). The nusselt number goes on increasing as the louver angle increases as can be seen from the figure. As the louver angle increases, the flow is disrupted to a greater extent as it tries to be alligned with the louvers. This increases the local heat transfer. Figure 2.13(b) shows that the performance enhancement factor is maximum for louver angle of 30° and minimum for a louver angle of 25°. Figure 2.14 shows that both normalized

temperature and pressure increase with an increase in wavy angle. Increased wavy angle poses greater obstruction for the flow and hence the increased pressure.

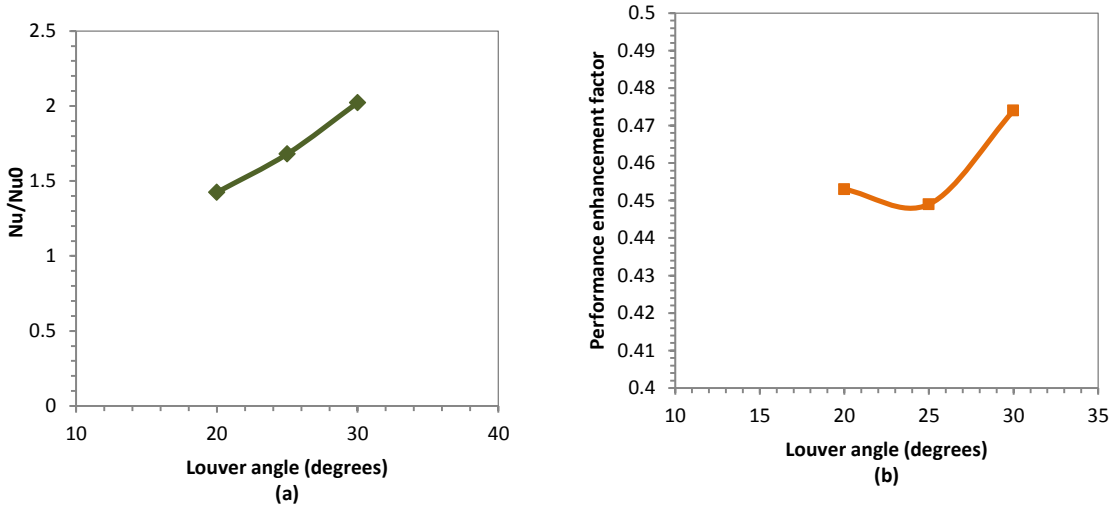

Fig. 2.13: (a) Variation in ratio Nu/Nu_0 with louver angle (b) Variation in PEF with louver angle

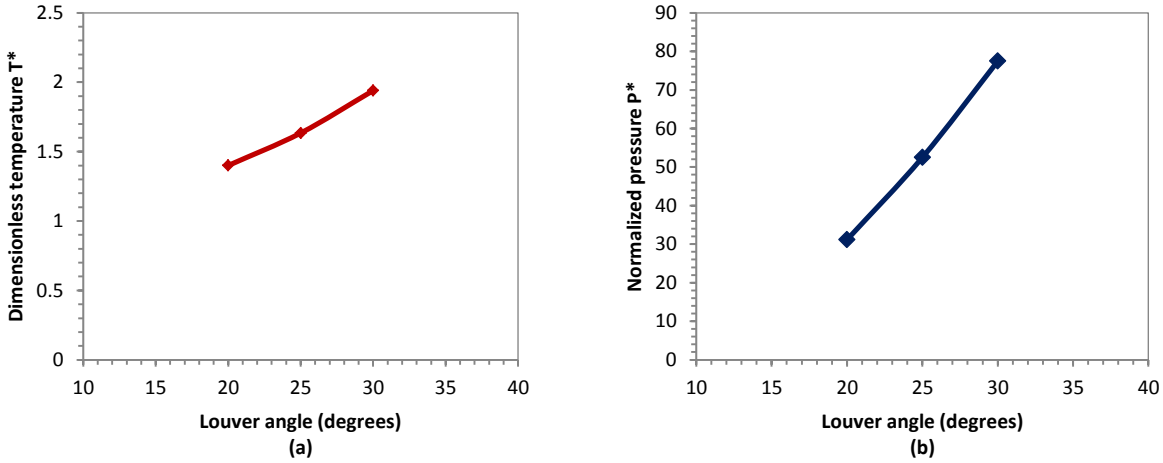

Fig.2.14: (a) Variation in dimensionless temperature with wavy angle (b) Variation in normalized pressure drop with wavy angle

2.4.5. Effect of varying Lp/Fp ratio:

Figure 2.15(a) shows the variation of relative nusselt number for Lp/Fp ratio varying from 0.925 to 1.823, the other parameters remaining constant ($\theta_l = 25°, Re = 10000$). In general, nusselt number increases with an increase in Lp/Fp ratio. This is because as the ratio Lp/Fp increases, either

by increase in louver pitch or by decrease in fin pitch, there is a relative decrease in resistance to flow in between the louvers as compared to the flow between the fins. This results in the flow being more louver directed than duct directed. Figure 2.15(b) shows that performance enhancement factor for varying Lp/Fp ratio is fairly constant.

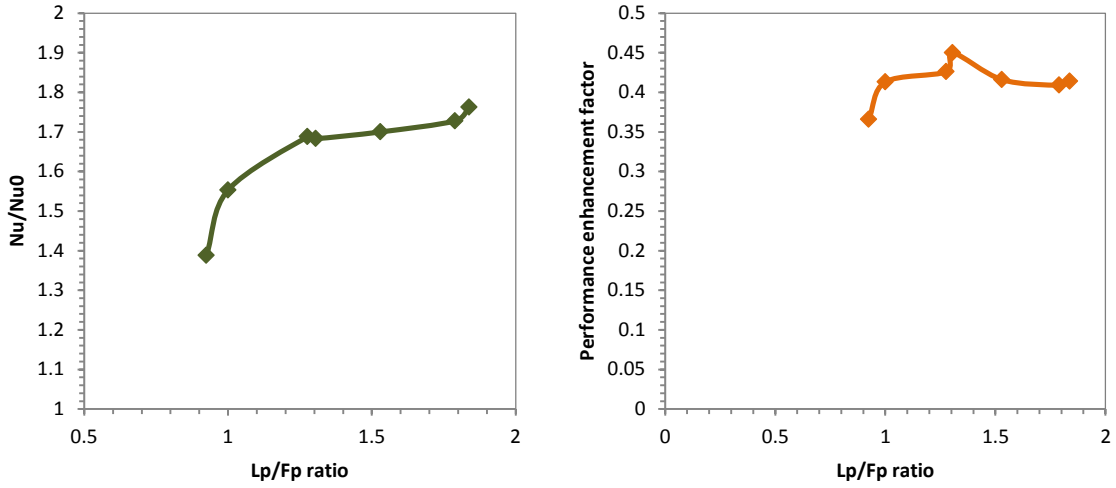

Fig.2.15: (a) Variation in ratio Nu/Nu_0 with variation in Lp/Fp ratio
(b) Variation in PEF with Lp/Fp ratio

Figure 2.16 shows the variation of normalized temperature and pressure drop as Lp/Fp varies. The pressure drop goes on increasing due to the increased disruption of flow as it becomes louver directed.

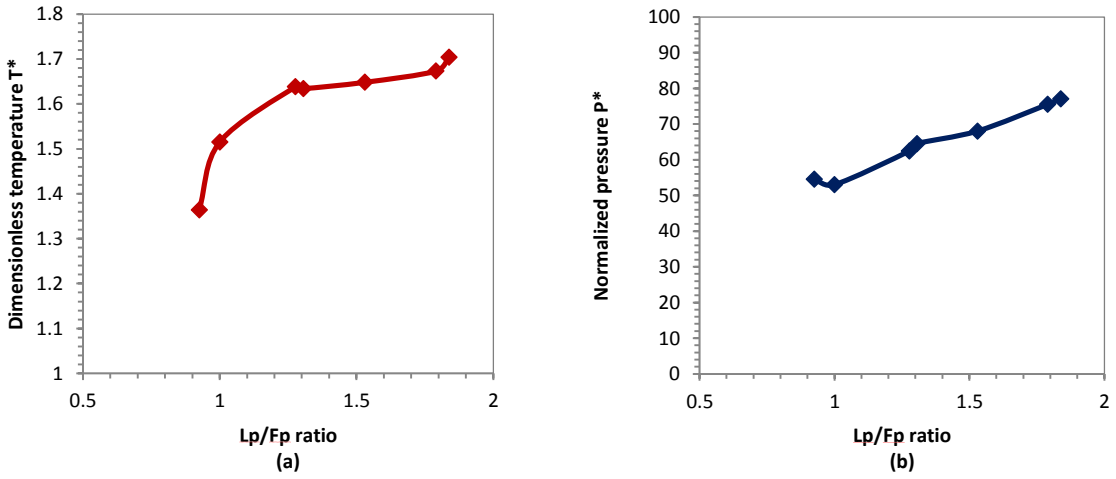

Fig. 2.16: (a) Variation in dimensionless temperature with variation in Lp/Fp ratio
(b) Variation in normalized pressure drop with variation in Lp/Fp ratio

CHAPTER 3: HERRINGBONE WAVY FINS

3.1 Literature Review:

Several studies on thermal and hydraulic characteristics of flow in a channel with herringbone wavy fins have been reported in literature. While the literature is populated with studies of flow in a single corrugated channel, the present work extends it to that of multiple wavy channels. Local and average heat transfer characteristics for corrugated channels were first reported by Goldstein and Sparrow [22] in 1976 using naphthalene sublimation technique, wherein the authors concluded that corrugated channels provide substantial heat transfer augmentation for turbulent flows but only marginal for laminar flows. In experiments performed by O'Brien and Sparrow [23] using water as the working fluid with Reynolds number ranging from 1500 – 25000, heat transfer rates that were 2.5 times than that for a parallel plate channel were obtained. Also, it was found that the pressure drop in the channel is solely due to inertial losses.

Most of the numerical studies presented in the literature, assume laminar and 2D flow conditions for channels with herringbone wavy fins. Amano 1985 [24-25] reported one of the first numerical studies for the friction factor and Nusselt number in a corrugated channel, the results were observed to be in good agreement with experimental results available at the time. Two dimensional numerical simulations for corrugated fins were conducted by Yang, et al. [26] using special Lam-Bremhorst low Reynolds number turbulence model ($Re = 100 - 2500$) for corrugation angles of $15°$ and $30°$. It was reported that as the wavy angle of the corrugated fins increases, the flow becomes turbulent at a lower Reynolds number. Numerical studies by Naphon [27-28] have demonstrated the temperature distribution and flow development in corrugated channels to be a function of the wavy angle and the channel height. Experimental and numerical studies by Islamoglu and Parmaksizoglu [29-30] have

shown that for a $20°$ corrugated channel the fully developed Nusselt number increases as the channel height increases. However, it was reported that a smaller channel height improved the overall performance when friction losses were considered. Experimental studies by Elshafei, et al.[31] over a Reynolds number range from 3220 to 9420 have shown that the effect of phase shift (relative arrangement of peaks and troughs) on heat transfer depends on the channel spacing and has a little effect on the pressure drop.

Numerical studies for wavy fin and tube heat exchanger in a 3D domain were considered by Bhuiyan, et al.[32] with different wavy angles for turbulent flow regime using the $k-\omega$ turbulence model. It was found that the heat transfer increases with an increase in the wavy angle but this is accompanied by a loss in efficiency as the pressure drop increases as well. Corrugated fins can have different wavy profiles – triangular, triangular with rounded corners and sinusoidal. Experimental and Numerical studies by Dong, et al. [33] in a 3D computational domain showed that variation in wavy fin profile has very little effect on the thermal-hydraulic performance.

Almost all the previous studies have analyzed flow in a single corrugated channel. The present research is focused on investigating the flow and thermal behavior in a channel with multiple corrugated fins. Also, one of the geometrical parameters that were varied in this study is the extent of the fins into the channel, which has not been previously investigated. Thus, the configurations explored are unique and as such no previous studies can be directly compared to it. However, the trends for pressure drop and heat transfer coefficient compare well with the existing literature for a single channel.

The following sections deal with the description of the physical test geometry of the exhaust pipe as well as the internal herringbone wavy fin configuration .The computational set up including the domain discretization, boundary conditions, turbulence model and grid independence is also discussed. In the results section the trends obtained for heat transfer and pressure characteristics are analyzed. Performance of the various configurations is compared by considering the performance

enhancement factor that characterizes the enhancement in heat transfer achieved and the associated pressure drop increment in the system.

3.2 Geometry Description:

3.2.1 Exhaust pipe geometry:

Figure 3.1 shows the basic geometry of the exhaust pipe test section with the herringbone wavy fins.

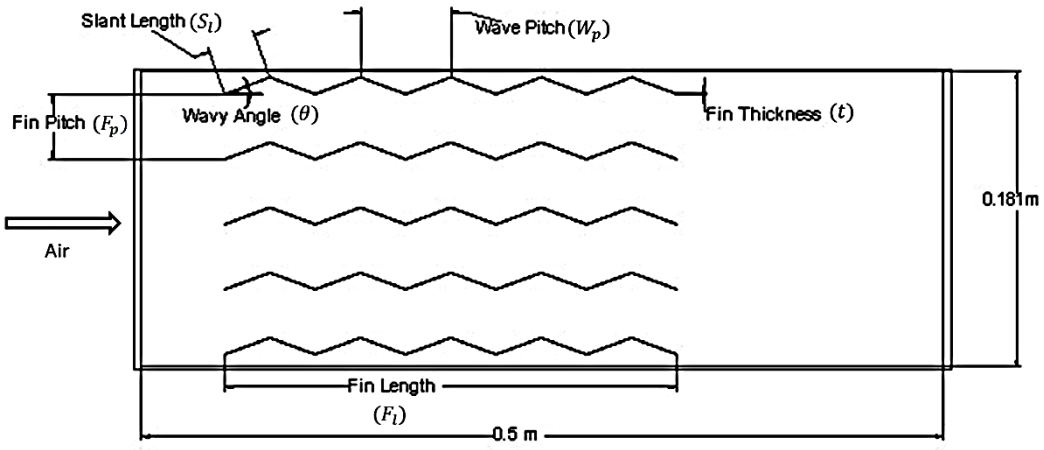

Fig.3.1: Basic geometry of test section with herringbone wavy fins

As shown in the figure the total length of the exhaust pipe test section is 0.5m. The exhaust pipe extends beyond the fin length on both sides to facilitate flow development and prevent back flow. The width is 0.181m and the depth into the paper is 0.0714 m. The thickness of this section is 0.003 and it is taken to have properties of steel.

3.2.2 Herringbone Wavy Fin Geometry:

The basic geometry of herringbone fins has been described in the introduction section. In incorporating them inside the exhaust pipe, each fin had five corrugation cycles. Thus the total fin length was $5W_p$ and which varied with the wavy angle. The fin thickness (t_l) was taken to be constant for all the configurations. While varying the geometric parameters the exhaust pipe dimensions are taken to be fixed.

Thermal and flow characteristics have been analyzed for variation in three parameters – wavy angle, Reynolds number and the extent of fins. Different wavy angles tested are - $20°, 22.5°$ and $25°$ and the Reynolds numbers tested are 10000, 20000 and 30000. Variation in extend of the fins was unique feature of this study which has never been explored before and hence is explained in greater detail below.

Figure 3.2(a) shows a three dimensional view of the test section with the front face being the inlet and the rear face being the outlet. Figure3. 2(b) shows the top and the side view to better represent the fins protruding from the two faces. The fins were alternately arranged on the two faces such that a fin on any one face is exactly half way between two fins on the opposite face.

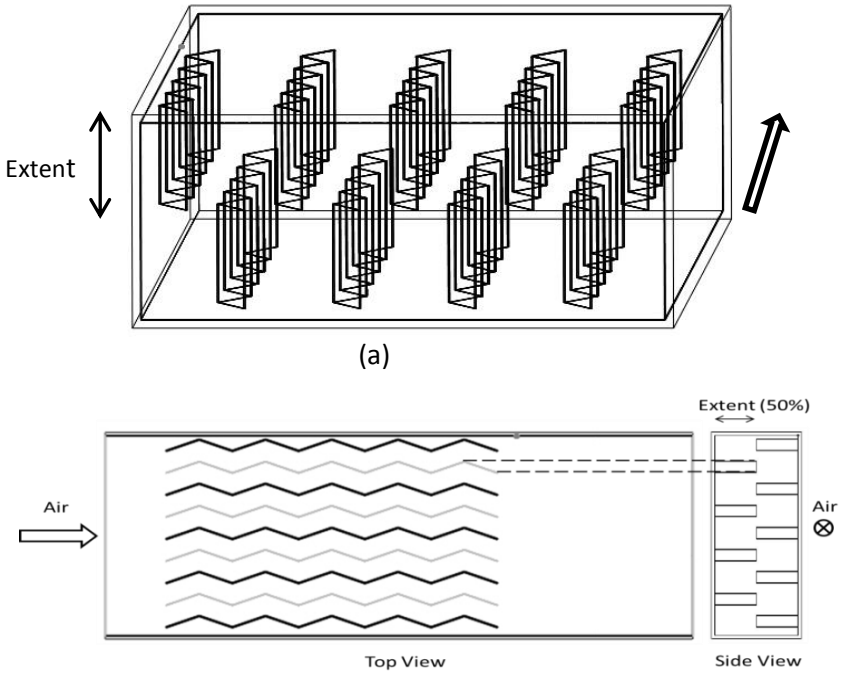

Fig.3.2. (a) Three dimensional view of the test section, (b) Top and side view of the test section

In Fig. 3.2 the fins extend to 50% of the channel height and hence there is no overlap between fins from the opposite faces. As this extend increases to 75% there would be an overlap and for the case

where the extent is 100% the exhaust pipe would basically be divided into 7 corrugated channels in the middle with two narrow channels on the sides.

Table 3.1 gives a list of all the parameters with their fixed or varying values:

Table 3.1. Geometrical parameters of test section with herringbone wavy fins

Parameter	Value
Length of test section(L)	0.5m
Width of test section(W)	0.181m
Height of test section(H)	0.0714m
Slant Length	0.03m
Fin thickness	0.0005m
Fin Pitch	0.04m
Wavy angle	20°/22.5°/25°
Wave Pitch	0.05638m/0.05543m/0.054378m
Fin length	0.2819m/0.2772m/0.2719m
Extent of fins	25%/50%/75%/100%

3.3 Computational set up:

The numerical simulations have been performed using the commercial CFD code ANSYS CFX 13.0 which uses the finite volume method for analysis. The 3D computational geometry was as per Fig. 3.1. with two domains – fluid domain defining the air flow region and the solid domain comprising the exhaust pipe shell and the fins. It is a conjugate heat transfer model taking both, the convection inside the fluid domain as well as the conduction within the fins and the exhaust pipe shell into account.

The fluid and the solid domain have been discretized using an unstructured grid comprising of tetrahedrons, pyramids and wedges using the patch conforming method. Figure 3.3 shows the details of the mesh.

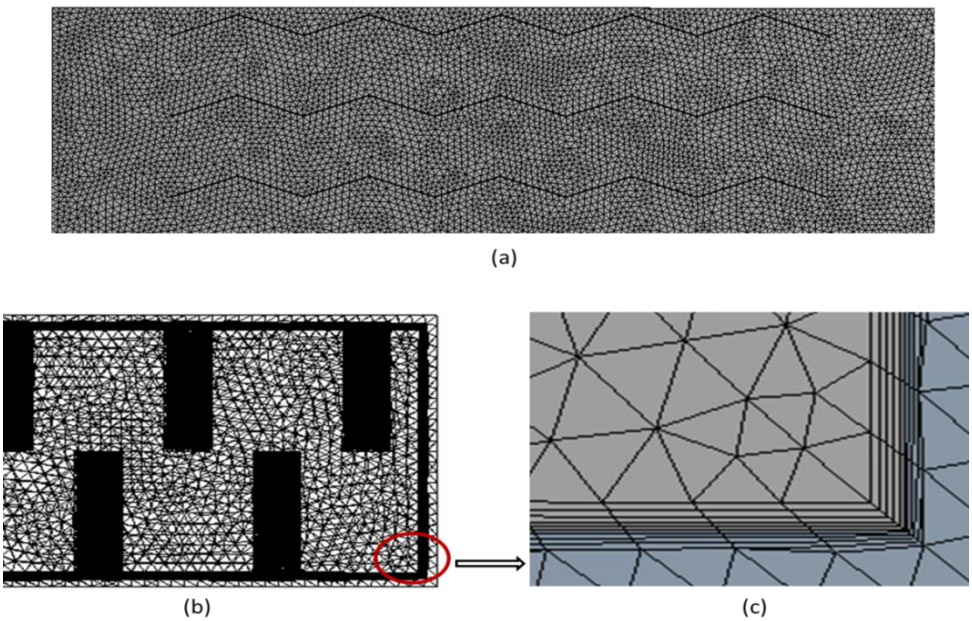

Fig.3.3: (a) Top view, patch conforming mesh (b) Discretization of the fluid and solid domain with inflation layers at the interface (c) Enlarged inflation layers

Inflation layers have been applied at the interface of the solid and fluid domain to effectively resolve the boundary layer as seen in Fig. 3.3(b) and 3.3(c). The first layer thickness for the inflation layers has been based off a Y^+ value equal to 1, which is the standard accepted value for the Shear Stress Transport Turbulence model. The first layer thickness is then given by[34]:

$$\Delta y = D_h Y^+ \sqrt{74} Re_{D_h}^{-13/14} \tag{3.1}$$

The working fluid was air (exhaust gases are modeled as air) [21] with ideal gas properties. Uniform velocity and temperature boundary condition has been applied at the inlet. The inlet temperature is taken to be 700K for all cases while the inlet velocity has been calculated based on the Reynolds number for each case. The outlet had a pressure boundary condition equal to atmospheric pressure. The solid domain (fins and exhaust pipe wall) has been assumed to be made of steel and has no slip boundary condition at the interface with the fluid. The outside of the exhaust pipe wall is modeled by applying a constant outgoing heat flux equal to $1000\ W/m^2$.

For all the three Reynolds number chosen the flow inside the exhaust pipe was turbulent. Industrial standard Shear Stress Transport (SST) model was employed to model the turbulence. The model uses the turbulence-based k- ω model at the wall and the k- ε model in the bulk flow with an automatic intermediate blending function that ensures a smooth transition between the two models [20]. It has been shown by studies that the solutions based on SST model are largely insensitive to the near wall grid resolution. The heat transfer from the fluid to the wall and thermal profile of the wall was an important metric for this study hence the SST model was found suitable.

The solution was considered to be converged when the rms value of the residuals dropped below 10^{-5} level.

3.3.1 Grid Independence:

To achieve a grid fine enough to be acceptable multiple simulations were carried out with varying mesh resolutions. Wall temperature and pressure drop are the metrics of interest and hence their variation were investigated for increasingly finer mesh to obtain a resolution for which the solution is independent of the grid. Figure 3.4 gives the variation for the wall Temperature and pressure drop with number of elements in the mesh. It can be observed that at a grid resolution of 2 million elements the solution becomes grid independent. The variation in results of temperature and pressure beyond this mesh level was found to be 0.148% and 0.56% respectively.

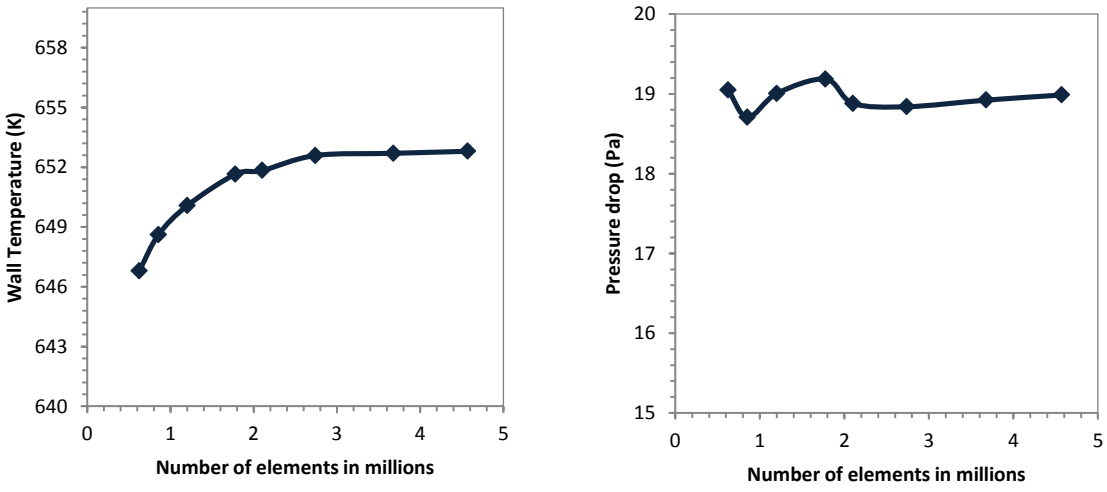

Fig.3.4: Variation in wall temperature and pressure drop with number of elements

3.4 Results and Discussion:

Numerical simulations have been performed to characterize the heat transfer and pressure drop in the exhaust pipe test section. The quantities of interest were the area averaged exhaust pipe wall temperature and the total pressure drop along the channel. Higher wall temperature is indicative of more heat being transferred from the exhaust gases to the walls and hence relates to higher heat transfer coefficient. Results are presented as normalized pressure drop and normalized wall temperature, calculated using the following normalizations:

$$P^* = \frac{\Delta p}{\Delta p_0} \tag{3.2}$$

$$T^* = \frac{T_{in} - T_0}{T_{in} - T_{w,avg}} \tag{3.3}$$

For the baseline case, $P^* = T^* = 1$

Average heat transfer coefficient is given by:

$$h = \frac{\dot{q}}{(T_b - T_{w,avg})} \tag{3.4}$$

Where, $\dot{q}$ is the applied heat flux boundary condition at the wall. The bulk fluid temperature is defined as:

$$T_b = \frac{T_{in} + T_{out}}{2} \tag{3.5}$$

$T_{w,avg}$ is the average surface temperature of the walls.

The Nusselt number, Nu, and Reynolds number, Re are given by:

$$Nu = \frac{hD_h}{k_{air}} \tag{3.6}$$

$$Re = \frac{\rho v D_h}{\mu} \tag{3.7}$$

The characteristic length is the hydraulic diameter which is computed as:

$$D_h = \frac{2HW}{(H+W)} = 0.1025\ m \tag{3.8}$$

Another important parameter used to compare the performance of different configurations of the herringbone wavy fins has been the performance enhancement factor (PEF) given as:

$$PEF = \frac{(Nu/Nu_0)}{(\Delta p/\Delta p_0)^{1/3}} \tag{3.9}$$

As can be seen from the equation, PEF characterizes the heat transfer enhancement achieved for increased penalty in terms of pressure drop.

3.4.1 Flow in Herringbone Wavy Fins:

Fig.3.5 shows the flow phenomenon in herringbone wavy fins. The waviness of the fins causes the streamlines to be deflected from their original path and get aligned with the slant faces of the fins. This increases the flow length and causes mixing of the fluid resulting in increased heat transfer and pressure drop as compared to the baseline case for the same Reynolds number. At higher Reynolds number secondary flows and vortices are observed as seen in enlarged view Fig.3.5 (b).

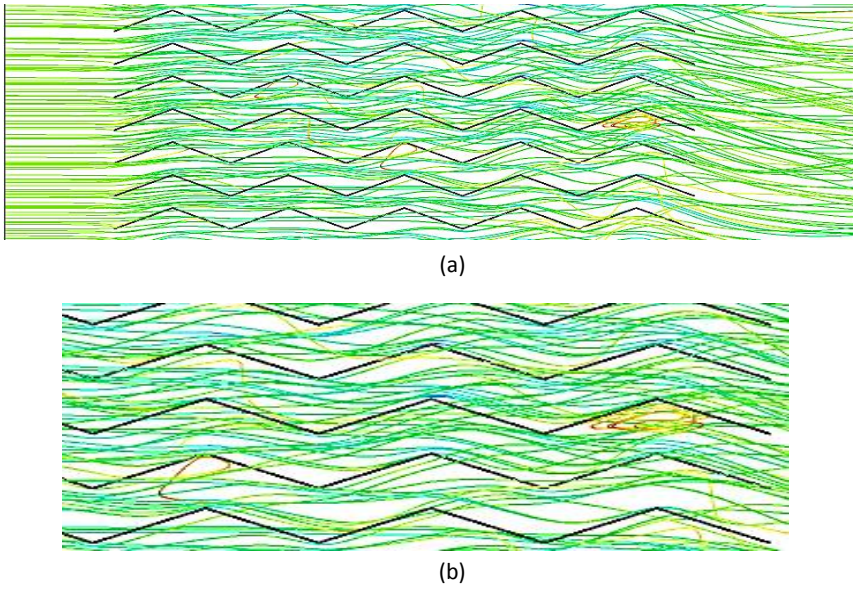

(a)

(b)

Fig.3.5: Streamlines for flow through herringbone wavy fins

3.4.2 Contour plots:

Figure.3.6 gives a representative comparison of wall temperature for the test section with herringbone fins with the baseline case. The geometric parameters for this fin configuration are shown in the figure. Flow through a channel with internal herringbone fins is characterized by higher convective heat transfer coefficient due increased residence time of the air in the channel and also because of destruction and reattachment of boundary layers. For the given contour plot the average wall temperature and heat transfer coefficient for the test section with the herringbone fins was found to be 652.586K and $22.3\,W/m^2$while for the baseline case it is 626.7K and $14.28\,W/m^2$. This indicates the potential of herringbone wavy fins for heat transfer enhancement for high Reynolds number.

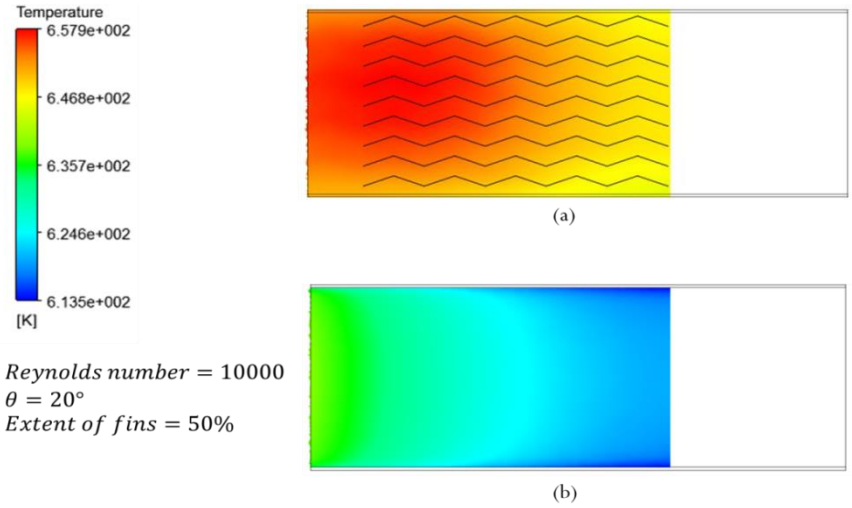

Fig.3.6: Comparison of wall temperature profile for herringbone wavy fins and baseline case

Figure.3.7 gives the comparison for the pressure drop for the herringbone fins with the baseline case. Internal fins are direct obstruction in the flow path and therefore result in a large increase in pressure drop. As expected, maximum pressure drop occurs when the flow first encounters the fins and almost all the pressure loss is confined to the section containing the fins with the pressure being fairly constant in the part of the channel with no fins. The total pressure drop for the test section with fins is 18.69 Pa while that for the baseline case is 2.082 Pa. The performance enhancement factor for this particular case is 0.752.

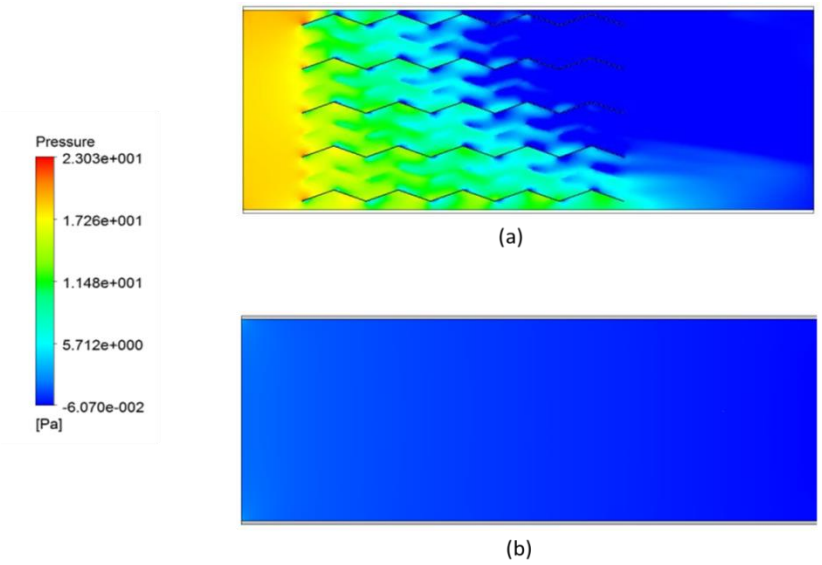

Fig.3.7: Comparison of pressure drop profile for herringbone wavy fins and baseline case

3.4.3 Comparison of 'in-phase' and '180° out of phase design':

Herringbone fins with two different relative fin arrangements have been tested for their flow characteristics. Figure. 3.8(a) shows the configuration where the fins are in phase with each other. Figure. 3.8(b) shows the configuration where the consecutive fins are 180° out of phase. Fig.3.9 (a) and 3.9(b) show the comparison of normalized temperature and pressure drop for these two configurations for three different wavy angles. It can be seen that there is only a slight difference in the heat transfer and pressure drop characteristics for the two fins. However, the in phase configuration proves to be comparatively more efficient as it has higher wall temperature enhancement at lower pressure drop. Thus the in-phase arrangement has been used for all the further simulations.

.

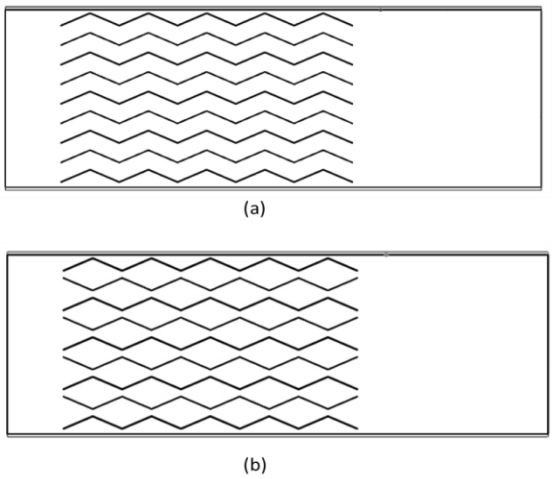

Fig.3.8: (a) Geometry of in-phase configuration (b) Geometry of '180 degrees out of phase configuration

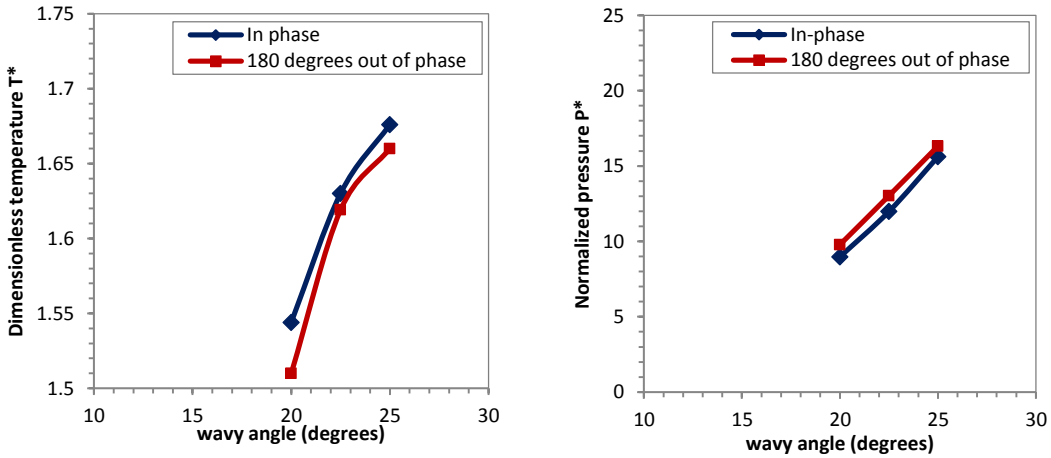

Fig.3.9: Variation in dimensionless temperature and normalized pressure for two fin configurations

3.4.4 Effect of Varying Reynolds Number:

Thermal and flow characteristics for the Herringbone wavy fins were investigated for three different Reynolds number (10000/20000/30000) while keeping the geometrical parameters fixed ($\theta = 25°, extent = 50\%$).

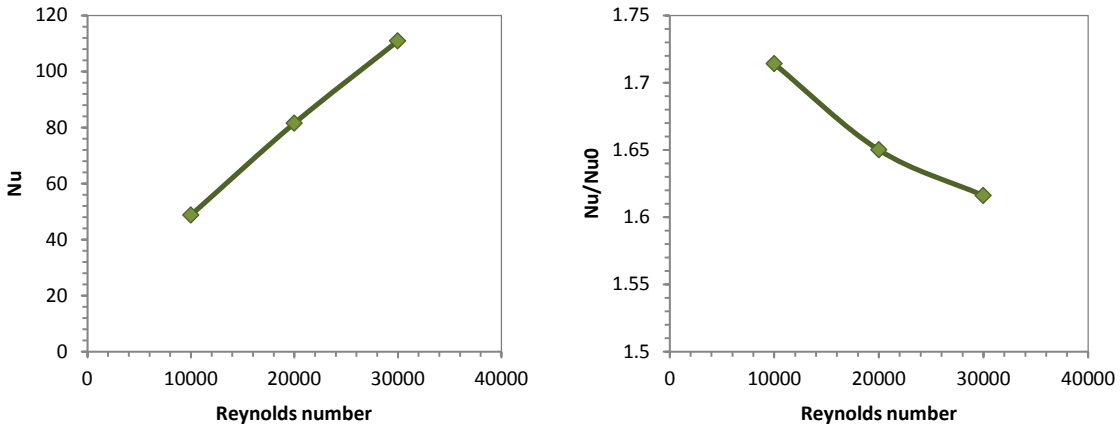

Fig.3.10: (a) Variation in Nusselt number with Reynolds number (b) Variation in ratio $Nu/Nu_0$with Reynolds number

Nusselt number is found to be highest for the case of Re=30000 and it decreases as Reynolds number decreases as seen in Fig. 3.10(a). This is because heat transfer is higher for increased mass flow rates associated with higher mass flow rates. However, the enhancement of heat transfer as compared to the baseline case decreases as the wall temperature approaches inlet air temperature. This can be seen in Fig. 3.10(b) where the ratio $Nu/Nu_0$is plotted against Reynolds number. Figure. 3.11 gives the normalized temperature and pressure drop as the Reynolds number is varied. It can be seen that pressure drop with respect to the baseline case increases rapidly as the Reynolds number increases. Curve for dimensionless temperature indicates that the difference $(T_{w,avg} - T_0)$is maximum for Reynolds number of 10000 and minimum for Re=20000.

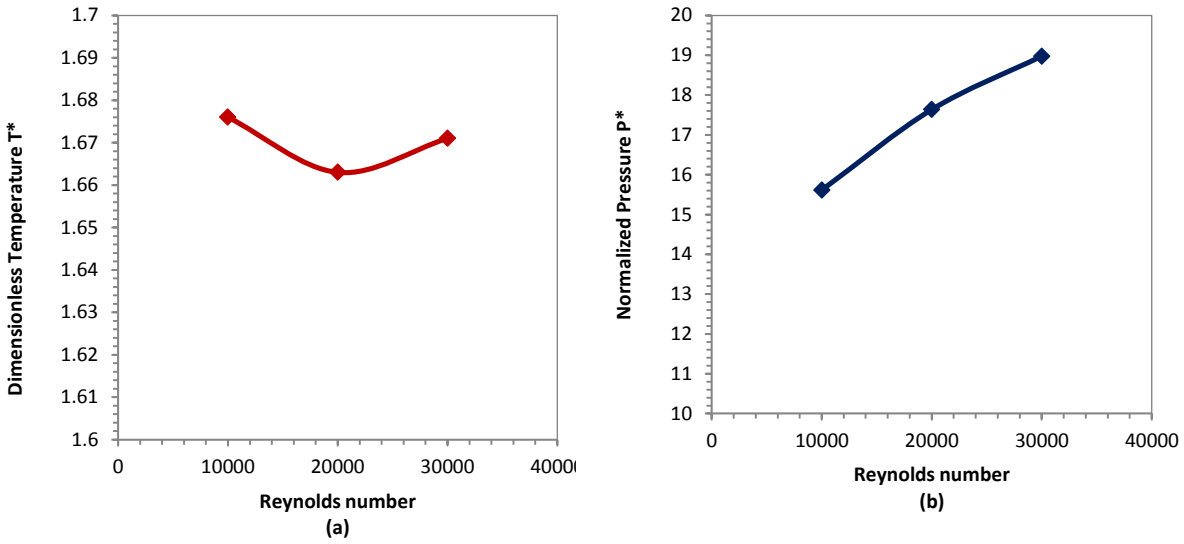

Fig.3.11: (a) Variation in dimensionless temperature with Reynolds number (b) Variation in normalized pressure drop with Reynolds number

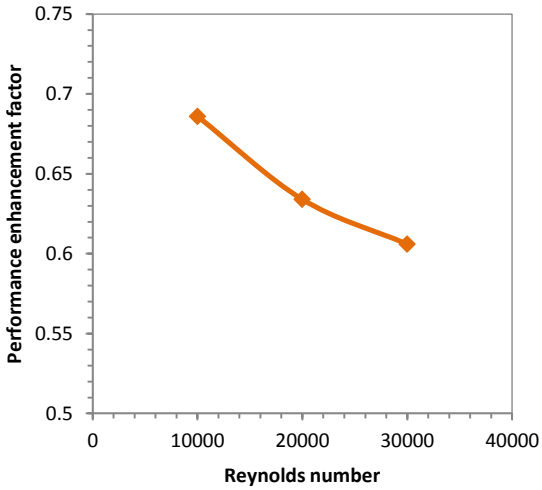

Fig.3.12: Variation in performance enhancement factor with Reynolds number

Figure 3.12 shows that the performance enhancement factor decreases as the Reynolds number increase due to exponential increase in the pressure drop**.** As expected, increased flow rate through the heat exchanger will required higher pressure drop through the device.

3.4.5 Effect of Varying Wavy Angle:

Figure.3.13(a) gives variation in relative nusselt number with varying wavy angle, the other parameters remaining constant ($Extent = 50\%, Re = 10000$). The nusselt number goes on

increasing as the wavy angle increases as can be seen from the figure. Increased wavy angle means increased disruption of flow, higher mixing and increased occurance of secondary flows and vortices which attribute to increase in convective heat transfer. All the three configurations tested were of the same fin pitch and hence the increase in heat transfer can be attributed to increase in the disruption of flow as it tries to be alligned with the fins with greater fin angle. Also as the number of corrugations in a single fin is kept constant for all the three configuration, the axial flow length is not constant as listed in table 1. Thus, it should be noted that for the same axial length, the fins with larger wavy angle will have greater number of corrugations and area and hence even greater heat transfer than what is reflected in Fig.3.13(a). Higher wavy angle poses greater obstruction to the flow. Moreover, as increase in wavy angle promotes secondary flows and local turbulent zones, it is associated with increase in pressure drop as seen in Fig. 3.14(b). Large increase in pressure drop through a channel with herringbone fins as the wavy angle increases explains the decreasing trend for PEF as seen in Fig. 13(b).

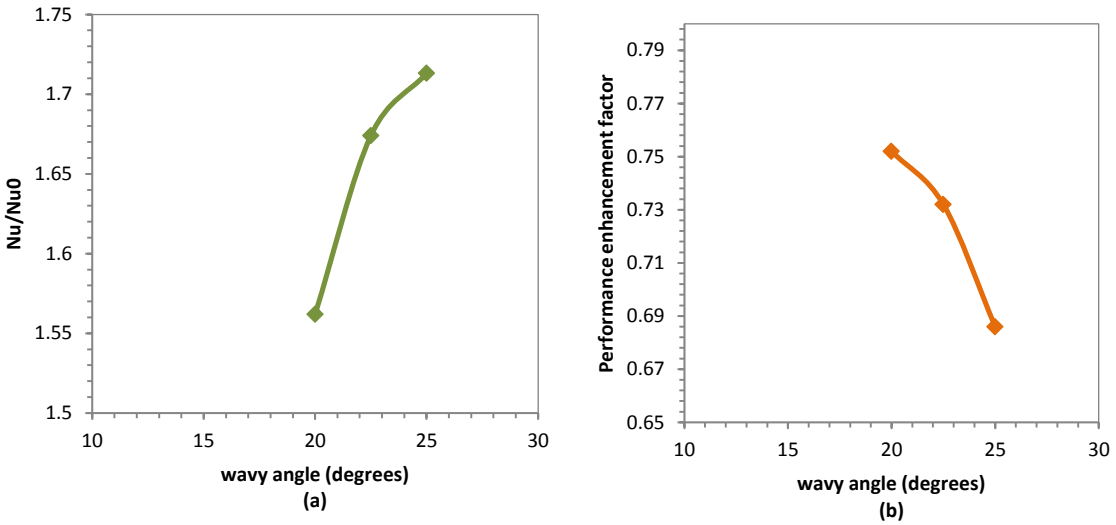

Fig.3.13: (a) Variation in the ratio Nu/Nu_0 with wavy angle (b) Variation in PEF with wavy angle

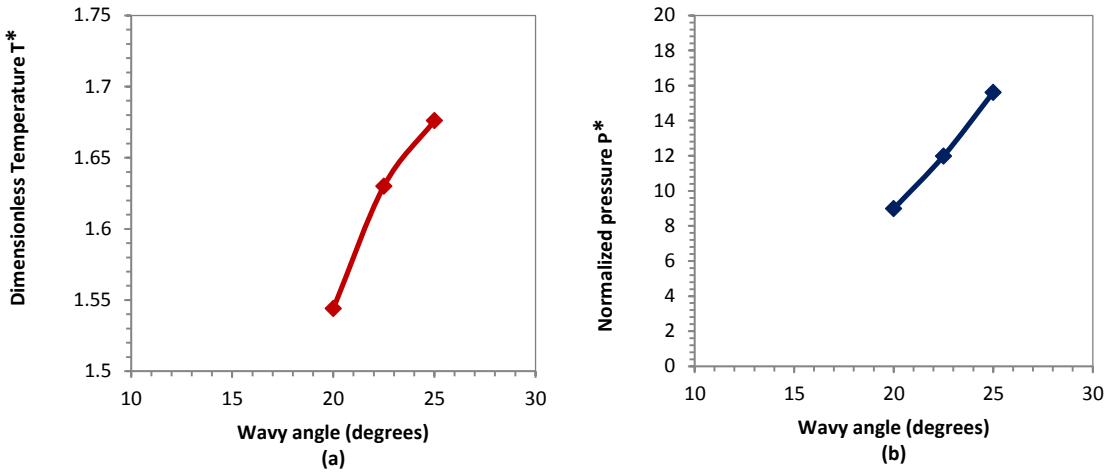

Fig.3.14: (a) Variation in dimensionless temperature with wavy angle (b) Variation in normalized pressure drop with wavy angle

3.5.6 Effect of Varying Extent of Fins:

Figure 3.15 (a) shows the variation of nusselt number for herringbone fins with varying extent of the fins perpendicular to the flow direction, the other parameters remaining constant ($\theta = 20°, Re = 10000$). Nusselt number is highest for the configuration where the fins extend to 50% of the channel width. When the extent is only 25%, the fluid in the central core of the duct is not disturbed by the fins at all and hence there is less recirculation and mixing. Also lower extent decreases the wetted surface area of the fins available for heat transfer and thus results in lower wall temperature. When the extent of the fins is 75% and for completely channelized flow (extent 100%), there is reduced or no mixing of air in the span wise direction as the air remains contained between the same set of fins. This explains the reduced heat transfer as compared to the configuration with extent=50%.

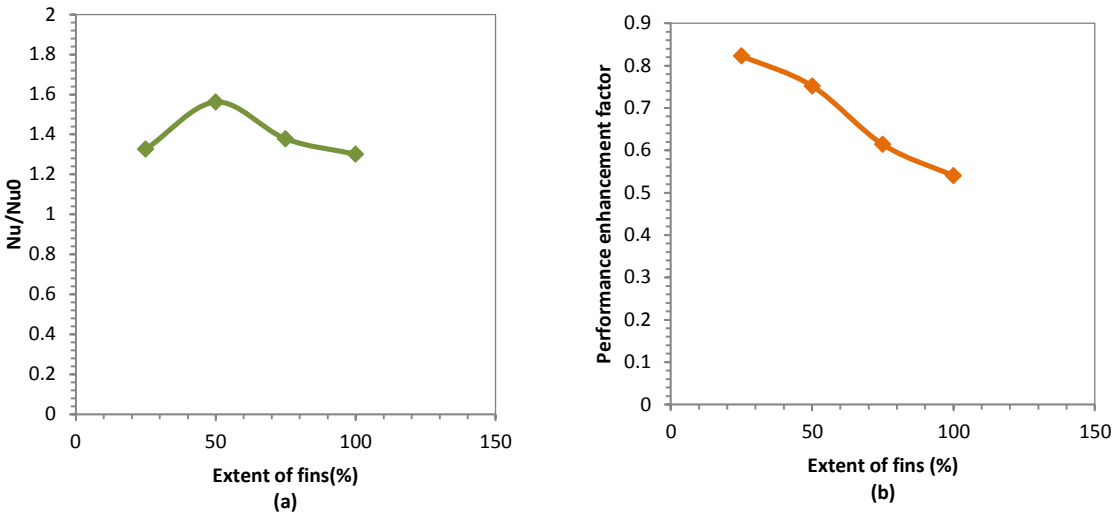

Fig.3.15: (a) Variation in the ratio Nu/Nu_0 with extent of fins (b) variation in PEF with extent of fins

Figure 3.16 shows the variation of normalized temperature and pressure drop as the extent of fins varies. Increase in extent of fins perpendicular to the flow direction essentially means increased blockage in the flow direction leading to an increase in the pressure drop. Also, for a part of the flow domains for 75% extent configuration, where the fins from opposite faces overlap, and also for the whole flow domain for the extent = 100% configuration, the effective fin pitch is half of that for 50% extent configuration. Thus air moves through narrower channels which increase the pressure drop as seen in Fig. 3.16(b).

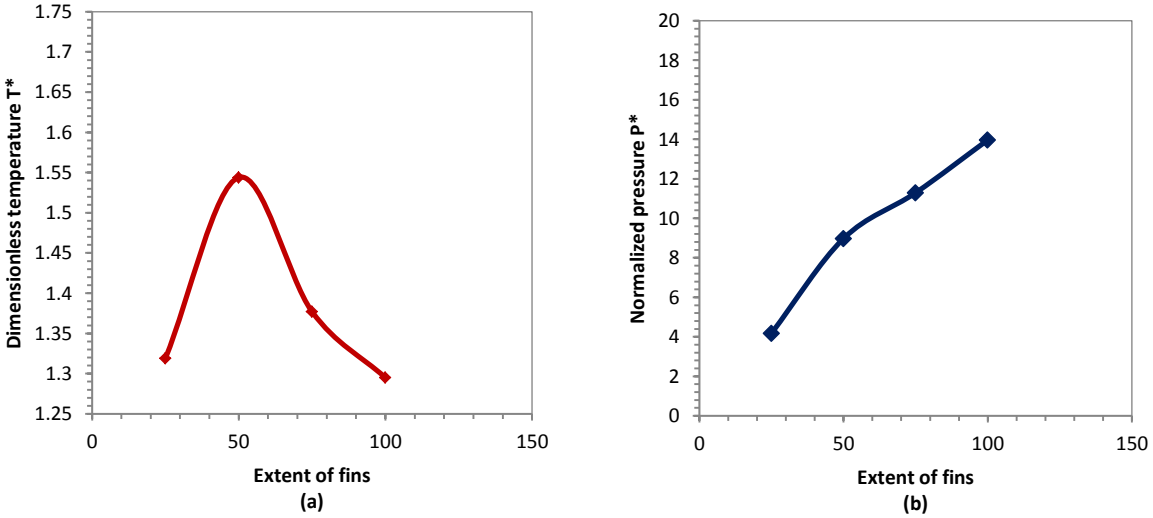

Fig.3.16 (a) Variation in dimensionless temperature with extent of fins (b) Variation in normalized pressure drop with extent of fins

4. COMPARISON BETWEEN LOUVERED FINS AND HERRINGBONE WAVY FINS

Louvered fins and herringbone wavy fins are fundamentally different in their geometry and hence cannot be directly compared. However, certain non-dimensional metrics for the two fins have been assessed to determine relative standing of the two fins in terms of performance, heat transfer enhancement and thermal characteristics at high Reynolds number.

4.1. Comparison of performance enhancement factor:

One of the major design considerations for internal fins is the amount of heat transfer enhancement achieved with respect to the penalty in terms of pressure drop. Performance enhancement factor is used to characterize this. Figure 4.1 gives the performance enhancement factors for all the configurations tested. The highest factor reached was 0.823 for the herringbone fins. It can be seen from the figure that, in general, herringbone wavy fins perform better than louvered fins.

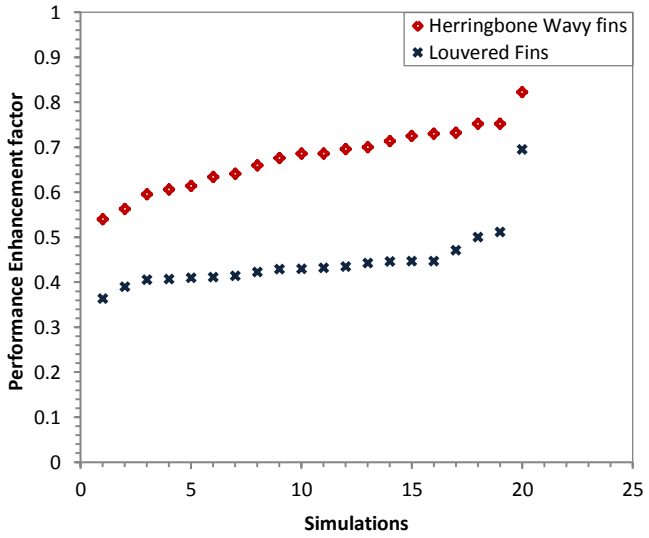

Fig.4.1: Comparison of performance enhancement factor

4.2 Comparison of Heat Transfer Enhancement at High Reynolds Number:

Figure 4.2 shows the relative nusselt number plots with varying Reynolds number for flow louvered fins and herringbone fins. It can be seen from Fig. 5.2 (a) that the relative nusselt number increases as the Reynolds number increases for louvered fins. This indicates that greater heat transfer enhancement is achieved for flow through louvered fins as Reynolds number increases. However, Fig 4.2(b) shows that for flow through herringbone wavy fins, the relative nusselt number and hence heat transfer enhancement achieved decreases as the Reynolds number increases. It can thus be concluded that louvered fins perform better at higher Reynolds number as compared to herringbone wavy fins.

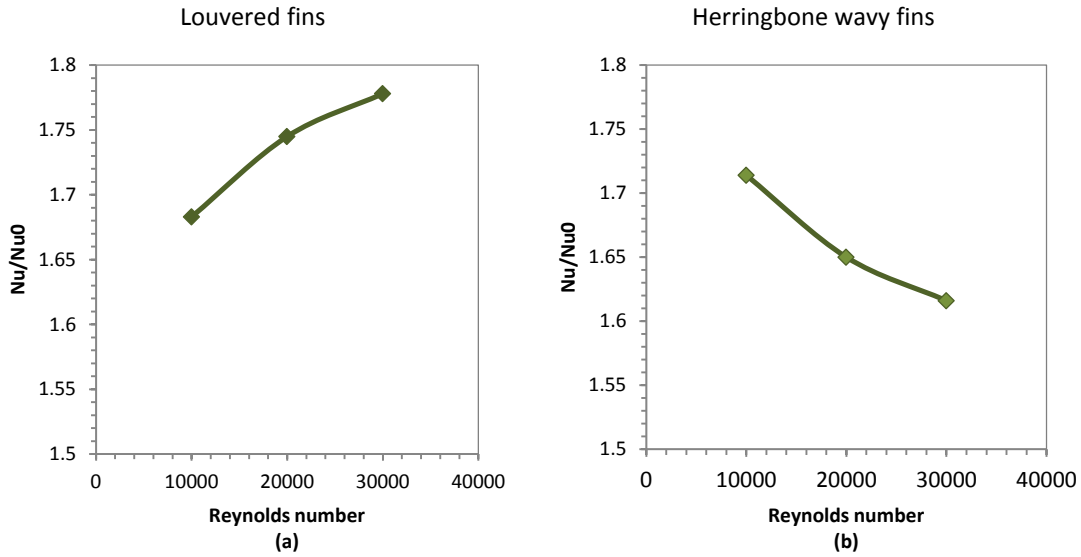

Fig. 4.2: (a) Variation in Nu/Nu_0 with Reynolds number with louvered fins
(b) variation in Nu/Nu_0 with Reynolds number with Herringbone wavy fins

4.3 Comparison of Configurations with Highest Heat Transfer Enhancement:

Trends for heat transfer enhancement with varying geometric parameters were used to design configurations for the two fins that could potentially give maximum possible heat transfer. Results for those configurations are given in the table 4.1.

Table 4.1: Comparison or metrics for the configurations providing highest heat transfer for the two fins

Parameter	Louvered Fins	Herringbone wavy fins
Nu/Nu_0	2.042	1.616
$\Delta p/\Delta p_0$	95.975	18.976
PEF	0.446	0.606

The geometric parameters for the above configurations for the two fins are:

Table 4.2: Geometric parameters for the configurations providing highest heat transfer for the two fins

Louvered Fins		Herringbone wavy fins	
Louvered angle	30°	Wavy angle	25°
Lp/Fp ratio	1.3055	Extent	50%
Reynolds number	30000	Reynolds number	30000

CHAPTER 5: GEOMETRY VALIDATION

For the purpose of geometry optimization of the internal fins, the exhaust pipe section has been modelled as a rectangular pipe which allows for easier manipulation of the geometric features of the internal fins. However, to make sure that the results obtained for the rectangular section can be extended to apply to exhaust pipe section as in Fig 1.1 simulations were carried for both the geometries using same boundary conditions. The inlet velocity has been scaled based on equal Reynolds number. The results heat transfer for both the cases match within 0.228 % and are presented in this section.

5.1 Streamlines:

For computational economy, only half section of the exhaust pipe section as in Fig 1.1 was modeled. The Reynolds number being high, the streamlines tend to be concentrated in the central core region without being diffused over the entire cross section of the channel. Baffles have been incorporated in the entrance region to facilitate uniform distribution of flow. The flow streamlines are shown fin Fig. 5.1.

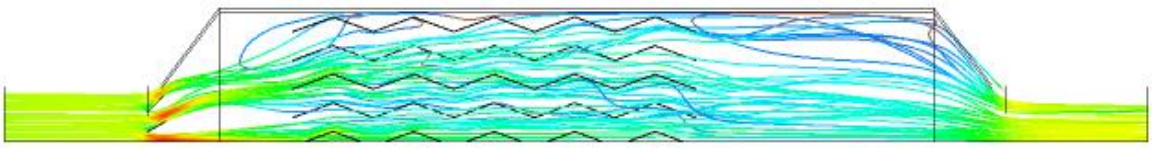

Fig. 5.1: Streamlines in exhaust pipe section

5.2 Wall temperature contour:

Figure 5.2 gives the temperature contour comparison for the rectangular exhaust pipe sections and the exhaust pipe section as in Fig. 1.1. It can be seen that there is no significant difference between the wall temperature contours. There is a slightly low temperature zone in the upper region in Fig. 5.2(b). This is expected due to the lower streamline density in that region as compared to through the central

core region. The average wall temperature for the rectangular exhaust pipe section is 652.586K while that for the section in Fig 5.2(b) is 651.1K

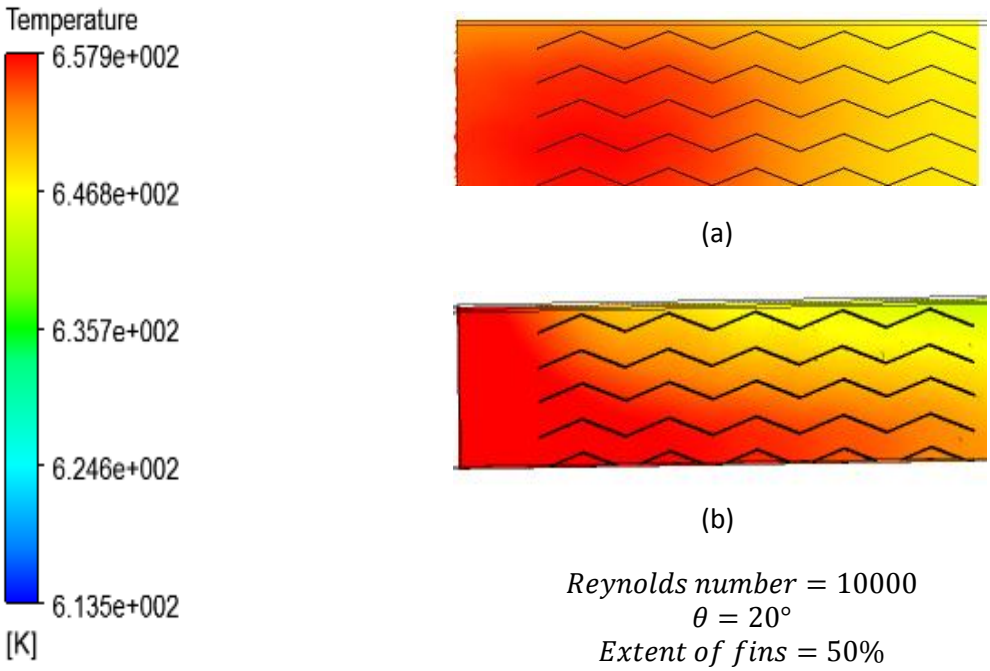

Fig.5.2: (a) Wall temperature contour for rectangular channel (b) Wall temperature contour for channel as in Fig. 1.1

CHAPTER 6: CONCLUSION

Numerical results of the present study indicate that louvered fins and herringbone wavy fins display great potential for heat transfer enhancement. However, the associated pressure drop increases as well. For the two fins trends for pressure drop and heat transfer characteristics show that –

Louvered Fins:

i. Increase in Reynolds number results in increase of the heat transfer as well as pressure drop for flow through louvered fins.

ii. Heat transfer and pressure drop increases as the louver angle for the louver fins increases.

iii. As the ratio Lp/Fp increases, heat transfer as well as pressure drop in a channel with louvered fins increases.

Herringbone wavy fins:

i. Increase in Reynolds number results in increase of the heat transfer as well as pressure drop for flow through herringbone fins.

ii. Heat transfer and pressure drop increases as the wavy angle for the herringbone fins increases.

iii. Maximum heat transfer is achieved for the 50% extent of the fins which decreases if this extent is increased or decreased. The pressure drop goes on increasing with the extent as the resistance to flow increases.

In general, herringbone wavy fins perform better than louver fins as seen from the trends for performance enhancement factor in fig. 4.1. This is majorly because of excessive pressure drop for flow through louvered fins as compared to flow through herringbone wavy fins. However, heat

transfer enhancement characteristics are better for louvered fins than herringbone wavy fins as Reynolds number increases.

This study dealt with a heat exchanger design for a specific application where large pressure drops can be sustained. As such the focus was to achieve the highest exhaust pipe wall temperature without much concern for the loss in pressure. On the basis of the above trends, various parameters were chosen to reach configurations which would result in highest wall temperature. The results and parameters have been given in section 4.3.

REFERENCES

[1] Hess, K.L., "The growth of automotive transportation", (1984)

[2] Yang, J. and Caillat, T, "Thermoelectric Materials for Space and Automotive Power Generation." *MRS Bull. 31*. pp 224-229,(2006)

[3] Yang, J. and Stabler, F. "Automotive applications of Thermoelectric Materials." *Journal of Electronic Materials*.38(7).(2009)

[4] Wojciechowski.K., Merkisz, J., Fuc P., Lijewski, P.Schmidt, M."Study of Recovery of Waste Heat from the Exhaust of Automotive Engine." Proc., 5th European Conference on Thermoelectrics. Odessa, Ukraine. (2007)

[5]Yang, J. "Potential Applications of Thermoelectric Waste Heat Recovery in the Automotive Industry." Proc. 24th Int. Conf. Thermoelectrics. Clemson University, United states. IEEE, 155-160. (2005)

[6] Vazquez, J., Sanz-Bobi, M., Palacios, R. Arenas, A. "State of the Art Thermoelectric Generators Based on heat Recovered from Exhaust gases of Automobiles." Proc.,7th European Workshop on Thermoelectrics.Pamplona, Spain, Paper no.17,(2002)

[7] Pandit, J., Dove, M., Ekkad, S., and Huxtable, S. "Heat Exchanger design for Waste Heat Recovery from Automobile Exhaust Using Thermoelectric Generators." *Proc., 50th AIAA Aerospace Sciences Meeting.* Nashville, Tennessee.

[8] Oates, G. C. (ed.), *Aerothermodynamics of Gas Turbine and Rocket Propulsion*, AIAA Education Series, AIAA, New York, pp. 19, 136,(1984)

[9] Gunnasegaran P, Shuaib N. H.,and Abdul Jalal1 M.F., "The Effect of Geometrical Parameters on Heat Transfer Characteristics of Compact Heat Exchanger with Louvered Fins", ISRN Thermodynamics, Volume 2012, Article ID 832708,2012

[10] Ali, M., M. and Ramdhyani, S., "Experiments on Convective Heat Transfer in corrugated Channels." *Experimental Heat Transfer: A Journal of Thermal Energy Generation, Transport, Storage, and Conversion*, 5(3), pp.175-193, (1992).

[11] Beauvais, F.N., "An Aerodynamic Look at Automotive Radiators", SAE Paper No. 650470, 1965.

[12] Wong, L.T. and Smith, M.C., "Air-Flow Phenomena in the Louvered Fin Heat Exchanger", SAE Paper No. 730237,1973

[13] Davenport, C.J., "Heat Transfer and Flow Friction Characteristics of Louvered Heat Exchanger Surfaces in *Heat Exchangers: Theory and Practice,* J. Taborek, G.F. Hewitt, and N. Afgan, Eds., Hemisphere, Washington, D.C., pp. 397-412,1983

[14] Achiachia, A., and Cowell, T.A., "Heat Transfer and Pressure Drop Characteristics of Flat Tube and Louvered Plate Fin Surfaces", Experimental Thermal Fluid Science 1, pp. 147-157, 1988

[15] Webb, R. L., and Trauger, P. , " Flow structure in the Louvered Fin Heat Exchanger Geometry", Experimental Thermal and Fluid Sciences,4, pp. 205-217,1991

[16] Tafti, D. K., Wang, G., Lin, W., "Flow Transition in a Multi-louvered Fin Array", International journal of Heat and Mass transfer, 43, pp. 901-919,2000

[17] D Zhang, X., and Tafti, D. K., " Flow Efficiency in Multi-Louvered Fins", International Journal of Heat and Mass Transfer, 46, pp. 1737-1750,2002

[18] Suga, A., and Aoki, H., "Numerical study on Heat Transfer and Pressure Drop in Multi-Louvered Fins", ASME/JSME Thermal Eng.,4, pp. 361-368,1991

[19] Perrotin, T., and Clodic, D.," Thermal-Hydraulic CFD Study in Louvered Fin-and-Flat-Tube Heat exchangers", International Journal of Refrigeration, 27, pp. 422-432,2004

[20] Innovative turbulence modeling : SST model in Ansys CFX – Technical brief

[21] Perry, R. H., "Perry's Chemical Engineer's Handbook". McGraw-Hill, New York, 4th edition (1984)

[22] Goldstein, Leonardo, Jr., and Sparrow, E. M., "Heat/Mass Transfer Characteristics for Flow in a Corrugated Wall Channel," *ASME Journal of Heat Transfer*, 91, pp. 187-195,(1977).

[23] O'Brien, J. E. and Sparrow, E. M., "Corrugated-Duct Heat Transfer, Pressure Drop, and Flow Visualization." *ASME Journal of Heat Transfer*,104,pp. 410-416, (1982).

[24] Amano, R. S., "A Numerical Study of Laminar and Turbulent Heat Transfer in a Periodically Corrugated Wall Channel." *ASME Journal of Heat Transfer*,107,pp. 564-569,(1985).

[25] Izumi, R., Oyakawa, K., Kaga, S., and Yamashita, H., "Fluid Flow and Heat Transfer in Corrugated Wall Channels," *JSME Journal*, 47, No. 416, pp. 657-665, (1981).

[26] Yang, L. C., Asako, Y., Yamaguchi, Y. and Faghri, M., "Numerical Prediction of Transitional Characteristics of Flow and Heat Transfer in a Corrugated Duct." ASME Journal of Heat Transfer, 119, pp. 62-69,(1997).

[27] Naphon, P. "Heat Transfer Characteristics and Pressure Drop in Channel with V Corrugated Upper and Lower Plates", Journal of Energy Conservation and Management, 48, pp. 1516-1524, (2007).

[28]Naphon, P. "Effect of corrugated plates in an in-phase arrangement on the heat transfer and flow developments", International Journal of Heat and Mass Tranfer, 51, pp. 3963-3971, (2008).

[29] Islamoglu, Y. and Parmaksizoglu, C., "The Effect of Channel Height on the Enhanced Heat Transfer Characteristics in a Corrugated Heat Exchanger Channel", Journal of Applied Thermal Engineering, 23, pp. 979-987, (2003).

[30] Islamoglu, Y. and Parmaksizoglu, C., "Numerical Investigation of Convective Heat Transfer and Pressure Drop in a Corrugated Heat Exchanger Channel", Journal of Applied Thermal Engineering, 24, pp. 141-147, (2004).
[31] Elshafei, E. A. M., Awad, M. M., El-Negiry, E. and Ali, A. G., "Heat Transfer and Pressure Drop in Corrugated Channels", Energy, 35, pp. 101-110, (2010).
[32] Bhuiyan, A. A., Sardul Islam, A. K. M. and Ruhul Amin, M., "Numerical Study of 3D Thermal and Hydraulic Characteristics of Wavy Fin and Tube Heat Exchanger", Frontiers in Heat and Mass Transfer, 3, (2012).
[33] Dong, J., Chen, J., Zhang, W. and Hu, J., "Experimental and Numerical Investigations of thermal-hydraulic performance in wavy fin-and-flat tube heat exchangers", Journal of Applied Thermal Engineering, 30, pp. 1377-1386, (2010).
[34] Ansys solver modeling guide